

2

Charles River Analytics Inc.

Technical Report No. R90222
DARPA Contract No. DAAHOI-91-R061

AD-A243 409



An Alternative Concept For Aeroassisted Orbit Transfers

Paul G. Gonsalves, Scott M. Allen, and Alper K. Caglayan

August 1991

91 1119 052

Prepared for:

Major R.J. Bonometti
Defense Advanced Research Projects Agency
1400 Wilson Boulevard
Arlington, Virginia 22209-2308

91-15926



~~91 8 29 064~~

91-5351

Table of Contents

1. Introduction	1
1.1 Technical Objectives	3
1.2 Technical Approach	3
1.3 Summary of Results	4
1.4 Report Outline	7
2. Application of AOTs to LightSat/TacSats	9
2.1 AOT Taxonomy	9
2.1.1 AOT Scenarios	9
2.1.2 Mission Requirements	11
2.1.3 Satellite Parameters	12
2.2 Analytical Results	12
2.2.1 Atmosphere Density Modeling & Variation	13
2.2.2 Problem Formulation	15
2.2.3 Inclination Stationkeeping	18
2.2.4 Rotation of Line of Apides	20
2.3 Trade Studies	22
2.3.1 Variation of Perigee Height	22
2.3.2 Variation of Eccentricity	23
2.3.3 Variation of Reference Area	26
2.3.4 Variation of Satellite Mass	29
2.3.5 Variation of Aerodynamic Coefficients	31
2.3.6 Trade Studies Overall Results	33
2.4 Feasibility Assessment of AOTs	34
2.4.1 Applicable AOT Scenarios	34
2.4.2 Feasibility Aspects	35
3. Neural Network Approach to AOT Guidance	38
3.1 Neural Net Guidance Objectives	38
3.2 Backpropagation Neural Networks	39
3.3 LightSat/TacSat Neural Net Guidance Development	41
3.3.1 Neural Net Guidance Trajectory Database	42
3.3.2 Neural Net Guidance Architecture Selection	49
3.3.3 Neural Net Guidance Training	52
3.3.4 Neural Net Guidance Evaluation	57
3.4 Feasibility Assessment of Neural Net Guidance	63
4. Summary, Conclusions, and Recommendations	65
4.1 Summary	65
4.2 Conclusions	66
4.3 Recommendations	68
5. References	70
Appendix A: Related Bibliography	71
A.1 Plane Change Maneuvers	71
A.2 Co-Planar Maneuvers	72
A.3 Miscellaneous	72

R90222

Charles River Analytics Inc.

List of Figures

Figure 2-1: Upper Atmosphere Density Profile	14
Figure 2-2: Density Variation with Latitude	15
Figure 2-3: Effect of Perigee Height Variation on Inclination	23
Figure 2-4: Effect of Perigee Height Variation on Apsidal Rotation	23
Figure 2-5: Effect of Eccentricity Variation on Inclination and Orbital Lifetime	24
Figure 2-6: Effect of Eccentricity Variation on Apsidal Rotation and Orbital Lifetime	24
Figure 2-7: Total Inclination Change Over Orbital Lifetime for Varying Eccentricity	25
Figure 2-8: Total Apsidal Rotation Change Over Orbital Lifetime for Varying Eccentricity	25
Figure 2-9: Effect of Reference Area Variation on Inclination	26
Figure 2-10: Effect of Reference Area Variation on Apsidal Rotation	27
Figure 2-11: Effect of Reference Area Variation on Orbital Lifetime	28
Figure 2-12: Effect of Reference Area Variation on Total Inclination Change and Orbital Lifetime ($e = 0.6$)	28
Figure 2-13: Effect of Reference Area Variation on Total Apsidal Rotation and Orbital Lifetime ($e = 0.6$)	29
Figure 2-14: Effect of Satellite Mass Variation on Inclination	30
Figure 2-15: Effect of Satellite Mass Variation on Apsidal Rotation	30
Figure 2-16: Effect of Satellite Mass Variation on Total Inclination Change and Orbital Lifetime ($e = 0.6$)	31
Figure 2-17: Effect of Satellite Mass Variation on Total Apsidal Rotation and Orbital Lifetime ($e = 0.6$)	31
Figure 2-18: Variation of Aerodynamic Coefficients with Altitude	32
Figure 2-19: Effect of C_I Variation on Inclination	33
Figure 2-20: Effect of C_I Variation on Apsidal Rotation	33
Figure 3-1: Backpropagation Neural Network	40
Figure 3-2: Back Propagation Processing Element	40
Figure 3-3: Neural Net Guidance Design Methodology	41
Figure 3-4: State Trajectories ($u_0 = 1.3$)	44
Figure 3-5: Control Trajectories ($u_0 = 1.3$)	45
Figure 3-6: State Trajectories ($u_0 = 1.45$)	46
Figure 3-7: Control Trajectories ($u_0 = 1.45$)	47
Figure 3-8: State Trajectories ($u_0 = 1.6$)	48
Figure 3-9: Control Trajectories ($u_0 = 1.6$)	49
Figure 3-10: I/O Set 1 and a Single Hidden Layer Interconnect Structure	50
Figure 3-11: I/O Set 2 with a Multiple Hidden Layer Interconnect Structure	51
Figure 3-12: C Profiles with Selected Training Data	53
Figure 3-13: Learning Rate of the Single Hidden Layer Networks	55
Figure 3-14: Learning Rate of the Multiple Hidden Layer Networks	56
Figure 3-15: Training and Open-Loop Performance Comparison	58
Figure 3-16: Open-Loop Control Performance	59
Figure 3-17: Closed-Loop I/O Set Comparison	59

Figure 3-18: Neural Guidance Closed-Loop Performance on the Nontraining Trajectory.....	60
Figure 3-19: Closed-Loop Final Inclination and Longitude	61
Figure 3-20: Maximum Lift/Drag Ratio with Noise ($u_0 = 1.45$).....	62
Figure 3-21: Optimal Control Performance Under Parameter Uncertainty.....	62
Figure 3-22: Neural Control Performance Under Parameter Uncertainty.....	63
Figure 3-23: Closed-Loop Control Law Performance Under Parameter Uncertainty	63

Accession For	
NIIS GRAAI	<input checked="" type="checkbox"/>
BTIC TAB	<input type="checkbox"/>
Unannounced	<input type="checkbox"/>
Justification	
By	
Distribution/	
Availability Codes	
Dist	Avail and/or Special
A-1	

1. Introduction

Recent research has indicated the potential benefits of aeroassisted orbital transfer (AOT) maneuvers. Using approximate closed-loop guidance laws and/or numerical optimization algorithms, researchers have demonstrated significant fuel savings with aeroassisted maneuvers over to purely propulsive maneuvers for both co-planar and planar transfers. This research focuses on currently envisaged transatmospheric vehicles and atmospheric-bearing spacecraft such as the National Aerospace Plane (NASP) and NASA's Aeroassisted Flight Experiment (AFE). Basic research is needed to investigate other potential applications of aeroassisted orbital maneuvers and to address the on-line implementation feasibility of such atmospheric trajectory/guidance schemes. In particular, there is a need to identify vehicle and orbital parameters/geometries that are the design drivers for allowing application of aeroassisted maneuvers and for determining overall transfer performance and fuel requirements. As for on-line implementation of transatmospheric guidance schemes, artificial neural networks offer an attractive alternative approach that may ameliorate the associated computational burdens and be readily adaptable to environmental uncertainties encountered during atmospheric maneuvers. In this study, we investigate and identify the possible application of aeroassisted maneuvers to other vehicle/mission elements, determine the basic design drivers, and formulate a specific scenario using a neural network approach to the on-line implementation of a guidance scheme.

Previous applications of aeroassisted orbital transfers have concentrated on two specific maneuvers: 1) a co-planar orbital transfer from a high Earth orbit (HEO) (e.g., geosynchronous) to a low Earth orbit (LEO); and 2) an orbital plane change with or without a decrease in orbital altitude. In these maneuvers, one or two impulsive burns are used to inject the vehicle into the atmosphere. Once in the atmosphere, the vehicle is controlled via modulation of lift and the bank angle. For the co-planar transfer case, the atmospheric portion is used to slow the vehicle down by converting kinetic energy into heat, while for a plane change (at the same orbital altitude) a minimum energy-loss gliding turn to heading is employed. Several other scenarios can be envisioned for possible application of aeroassisted maneuvers. For instance, the more general case involving elliptical orbits is readily apparent, or more specifically transfers involving high inclination highly eccentric orbits (e.g., Molniya orbits). Other potential applications include using aerobraking for lowering orbital altitudes of LEO satellites, and designing spacecraft/booster systems to allow for high atmospheric flight. The latter design effort involves determining vehicle lift

requirements and heat transfer limits as well as obtaining an atmospheric guidance scheme. From such a design effort, the need for reconfigurable spacecraft may arise, that is, a spacecraft that has both an on-orbit and an atmospheric-bearing configuration. The use of such aeroassisted maneuvers could augment current spacecraft/booster systems in operation by making them more maneuverable and more fuel efficient. Future systems could benefit by incorporating knowledge gained by analyzing the requirements and design drivers for transatmospheric flight.

The optimum trajectory/guidance optimization for a transatmospheric vehicle requires the solution of a two-point boundary value problem with state and control constraints. Variational calculus yields a set of nonlinear differential equations for the state and co-state vectors as necessary conditions of optimality with split boundary values and en route constraints. The numerical solution of the necessary conditions is not a trivial task using current numerical techniques due to the stability characteristics of the co-state equations, and the sensitivity to parameter changes. While off-line solutions are feasible using efficient numerical algorithms such as multiple shooting, on-line numerical solutions remain unattainable. However, we assume that a suitable database of optimum guidance trajectories is available since significant recent research has focused on obtaining better numerical algorithms for obtaining these optimum trajectories. Our proposed on-line implementation approach is the neural network modelling of such an optimum trajectory/guidance database in order to obtain a closed-loop guidance law. Neural networks represent a nonalgorithmic class of information processing for using massively parallel distributed processing architectures. A neural net structure is a network of processing elements connected through information links. Each processing element is a multi-input/single-output dynamic system described by a first-order nonlinear differential equation.

Artificial neural networks produce a nearest-neighbor classifier. Conceptually, artificial networks are applicable to aeroassisted guidance problems for learning the spatiotemporal attributes of optimum guidance/trajectories for a given class of problems. Once the neural network is trained with an optimum trajectory/guidance database, then it can be used on-line to generate optimum guidance commands adapting to the uncertainties of the atmospheric flight operations. Such a neural network based guidance approach would be the nonalgorithmic counterpart to finding closed-loop guidance laws using algorithmic methods such as singular perturbation theory or energy state approximations. Given the emergence of recent fast, relatively inexpensive VLSI designs for realizing neural network

structures, the implementation of neural net based space vehicle guidance systems will soon become feasible.

1.1 Technical Objectives

The primary objectives of the effort reported here are to investigate possible applications of aeroassisted orbital transfers and to evaluate the feasibility of an on-line neural network implementation of an atmospheric trajectory/guidance scheme. The effort addresses the following basic questions:

- What are possible applications of aeroassisted orbital transfer maneuvers and what benefits may accrue from these applications? What are the vehicle and orbital design drivers that may preclude using aeroassisted maneuvers, and can these drivers be ameliorated? What constraints/requirements need to be imposed on future systems to allow use of aeroassisted maneuvers (e.g., aerodynamic)?
- How can we implement and evaluate aeroassisted orbital transfer concepts in a suitable and timely manner? Will such an implementation allow for proper postulation of these concepts and identification of design drivers?
- What are the most suitable trajectory/guidance schemes and what specific design trades should be considered? Can we generate a suitable trajectory/guidance database for training a neural network for use in a space vehicle guidance system?
- What is the appropriate artificial neural network architecture for modelling an optimum trajectory/guidance database? In particular, what are the network inputs/outputs, the complexity of the processing elements, and the interconnect architectures? Can we incorporate our a priori knowledge about the optimization solution into the neural network architecture?
- How can we demonstrate the feasibility of implementation of a neural network based optimum guidance approach?

1.2 Technical Approach

Our general technical approach to evaluate alternative aeroassisted orbital transfer concepts and to demonstrate feasibility of an on-line neural network implementation of an

atmospheric trajectory/guidance scheme centers on: 1) identification of aeroassisted orbital transfer concepts applicable to the LightSat/TacSat community; 2) the performance of trade studies to evaluate feasibility of these concepts and to determine key concept design drivers; 3) formulation and evaluation of neural network implementation for a given AOT trajectory/guidance database; and 4) propose follow-on design objectives and development paths for a specific LightSat/TacSat implementation and validation effort.

The first step in researching alternative aeroassisted orbital transfer concepts is the identification of all possible functional uses of such concepts. This requires the determination of vehicle/mission elements that may be enhanced through the use of aeroassisted maneuver concepts. Consideration is given to classifying the types of vehicles/missions that are or could be capable of aeroassisted maneuvers (e.g., small satellites in LEO, reconnaissance spacecraft in Molniya orbits, or polar sun synchronous satellites). Next, for these vehicles a determination of how can aeroassisted maneuvers enhance or augment mission effectiveness or prolong mission lifetime is required. This involves identifying specific mission orbital requirements, i.e., inclination stationkeeping, perigee location, satellite relocation, etc. Finally, the satellite parameters that play key roles evaluating feasibility of AOTs are identified.

The second step in this research effort is the performance of trade studies to determine the overall design drivers. Included in these studies is the analysis of both vehicle configuration/constraints and overall mission requirements. For a given concept and satellite, we look at the vehicle characteristics such aerodynamic coefficients, mass properties, physical characteristics, etc. Also studied are performance benefits obtained including enhanced mission effectiveness, increased mission lifetime, etc.

The third step of our effort is the formulation and evaluation of neural network architectures for an AOT guidance concept. In particular, various interconnect architectures and processing elements will be considered to incorporate the known attributes of the optimum guidance solution. The networks are trained on trajectories developed and then are evaluated on its on-line performance in classifying the optimum trajectories, approximating the optimal solution, satisfying end conditions, and coping with environmental uncertainties.

1.3 Summary of Results

The primary results of this study are the identification of possible new applications of aeroassisted orbital transfers to LightSat/TacSats and the feasibility evaluation of an on-line

neural network implementation of an atmospheric trajectory/guidance scheme. The major findings of this effort are summarized in the following paragraphs.

AOT scenarios can be classified into 2 distinct categories: on-orbit multiple-pass "soft maneuvers" and the single-pass deep penetration into the atmosphere "hard maneuver". Due to propellant limitations, the soft maneuver is very conducive to address LightSat/TacSat orbital transfer requirements. Possible soft-maneuvers include inclination and perigee location stationkeeping. Hard maneuvers are more conducive to situations requiring a greater amount of maneuverability, e.g., emergency relocation of a satellite.

Associated with each class of AOTs are a set of relevant vehicle and mission requirement parameters. This set of parameters help define the overall feasibility of AOTs. Chief among these parameters is perigee altitude. Perigee altitude determines the amount of atmospheric density available to perform on-orbit maneuvers. Density is seen to decrease exponentially with altitude such that AOTs are not feasible beyond a perigee altitude of 200 km. Lower perigee altitudes come with a detrimental effect of shorter orbital lifetimes. This can be ameliorated via more eccentric orbits. Among the relevant vehicle parameters are satellite mass, reference area, and aerodynamic efficiency.

Trade studies were performed for two specific soft maneuvers: plane change and rotation of line of apsides. Approximate sub-optimal expressions for plane change and apsidal rotation per revolution were derived. Parameters of interest were then varied with the following results:

- Variation of perigee height shows orders of magnitude increase in maneuver capability per revolution when going from 200 km to a 100 km perigee height due to increasing atmospheric density. Such an increase in maneuver capability is offset by the low orbital lifetimes at such altitudes, especially for low eccentricities.
- The amount of plane change and apsidal rotation per revolution decreases with increasing eccentricity. However, higher eccentricity has a beneficial effect on on-orbit lifetime. The decrease in plane change is by a factor of two over the eccentricity range of 0.1 to 0.6 with lifetime increasing by an order of magnitude from about 10 days to almost one year. Apsidal rotation per revolution decreases initially with increasing eccentricity, as with plane change, but then flattens out at higher eccentricities while lifetime increases. Higher

eccentricity orbits not only have a longer lifetime, but over the total lifetime achieved a greater total amount of plane change and apsidal rotation.

- An increase in satellite reference area has a beneficial effect on plane change and apsidal rotation per revolution while orbital lifetime is decreased. Since reference area linearly increases maneuver amount and linearly decreases orbital lifetime, the total maneuver amount over the lifetime is constant over the range of reference area with all other parameters held fixed.
- Mass decreases plane change and apsidal rotation per revolution with a concomitant beneficial effect on orbital lifetime. Lower mass, while producing a greater plane change and rotation per revolution, comes with lower lifetime cost, that is, a greater amount of maneuver is accomplished faster with smaller masses but with total orbital change over lifetime equal for all masses.
- Variation of vehicle aerodynamic coefficients with altitude were accomplished via exponential curve fits to common values encountered at perigee heights of 200 and 100 km. As a function of perigee height, results show orders of magnitude decrease in plane change and apsidal rotation per revolution with increasing altitude due to density and lift coefficient reduction. The results are comparable with those presented on perigee height variation with the superimposition of the effect of aerodynamic coefficient variation. These results further the necessity for performing maneuvers at lower altitudes.

Two AOT scenarios have demonstrated feasibility based on results of the trade studies. These are the inclination and rotation of line of apsides on-orbit stationkeeping maneuvers. For a 25 kg satellite with a perigee height of 150 km and an eccentricity of 0.6, a total lifetime plane change of over 3 degrees and a total apsidal rotation of over 5 degrees were demonstrated. Plane changes of 20° and higher become possible for lower perigee heights and with more aerodynamical efficient satellites. Possible applications of these maneuvers include stationkeeping for a satellite with a near-equatorial perigee location or compensating for rotating argument of perigee for satellites at near Molniya orbits. Other possible AOT scenarios include orbit circularization via the multi-pass maneuver, and the controlled deorbit of a satellite to prolong orbital lifetime or to relocate the satellite to deorbit over a strategic geographic region.

We have generalized our neural guidance approach (Caglayan and Allen (1990)) to deriving closed-loop LightSat/TacSat AOT guidance laws. Several neural network

interconnect structures were trained off-line with a database of guidance/trajectory solutions computed using a numerical optimization algorithm. The known characteristics of the optimal solution were used to determine two sets of network inputs and outputs. The on-line realization of the trained neural guidance laws generates the real-time guidance commands based on current measurements and initial constraints. The training, open-loop, and closed-loop performance of the neural guidance networks were evaluated with the following results:

- A backpropagation neural network can be trained to model the optimal guidance solution for the multi-pass plane change maneuver. The performance of the neural guidance law closely matches that of the optimal guidance law. In the presence of parameter uncertainty, the neural guidance law outperforms the optimal guidance law.
- A priori knowledge about the optimal solution can be incorporated into the neural network architecture. Networks with like interconnect structures trained to acceptable levels using the two different sets of inputs/outputs.
- Choice of network inputs impacts the rate at which the network learns the functional relationships required to predict the desired control commands. One set of inputs/outputs consistently produced better training performance over all network interconnect structures than the other set of inputs/outputs.
- For the multi-pass plane change maneuver, a multiple hidden layer network learns the desired controls faster than a single hidden layer network. For either input/output set, a given multiple hidden layer network reached a lower RMS error in a fewer number of training cycles than a given single layer network.

1.4 Report Outline

This report summarizes and documents our investigation of the application of AOTs to LightSat/TacSats and feasibility assessment of on-line ANN implementation of guidance schemes for such spacecraft.

Chapter 2 presents results pertaining to application of AOTs to LightSat/TacSats. Section 2.1 begins by classifying and discussing the various AOTs possible and the related mission and satellite parameters that directly relate to feasibility. Analytical results are next presented on section 2.2 for two possible scenarios. Section 2.3 details the trade studies performed. Section 2.4 concludes with a discussion of overall feasibility of AOTs.

Chapter 3 details the neural network approach to AOT guidance. Section 3.1 discusses the objectives of using a neural network approach to developing closed-loop guidance laws. Section 3.2 presents an overview of the backpropagation neural network paradigm used to develop the neural net guidance laws described in this report. The development of a closed-loop neural network guidance law for a specific AOT is detailed in section 3.3. Feasibility issues are then discussed in section 3.4.

Chapter 4 concludes the report with a summary, conclusions, and recommendations for future work.

2. Application of AOTs to LightSat/TacSats

In this chapter we present results pertaining to application of AOTs to LightSat/TacSats. We begin by classifying and discussing the various AOTs possible and the related mission and satellite parameters in section 2.1. We next present some analytical results for two possible scenarios in section 2.2. Section 2.3 details some relevant trade studies performed. Section 2.4 concludes with a discussion of overall feasibility of AOTs.

2.1 AOT Taxonomy

As part of determining feasibility of aeroassisted orbital transfers (AOTs) to LightSat/TacSats, we begin by classifying the various AOT scenarios, determining the mission requirements of LightSat/TacSats as they pertain to AOTs, and discussing the vehicle parameters that directly influence feasibility.

2.1.1 AOT Scenarios

Aeroassisted orbit transfers can be accomplished via two scenarios: a multiple pass orbit transfer or a single pass that involves a deep penetration into the atmosphere. We discuss both of these scenarios and the various types of orbit transfers capable of being performed.

Multiple Pass AOTs ("Soft Maneuver"):

The multiple pass aeroassisted orbital transfer, or "soft maneuver," involves allowing the vehicle to stay at higher altitudes and using available aerodynamic forces during each perigee pass to perform an orbital transfer. A typical scenario may begin with a deboost from the initial orbit into an elliptical transfer orbit with a perigee height within the effective atmosphere. After the desired atmospheric maneuver has been accomplished, a reboost to the final orbit is performed. The requirements for boosting and deboosting may be waived if the initial perigee height is within the effective atmosphere. The major advantages of the soft maneuver are that it may be performed on-orbit and thus may not require deboost and reboost burns, and it encounters low heating rates and acceleration levels. The advantages make the soft maneuver very conducive to application to stationkeeping for LightSat/TacSats. The major drawbacks include overall time to perform the maneuver and the feasibility of certain scenarios given the low aerodynamics forces encountered at orbital altitudes.

For a plane change soft maneuver beginning from an eccentric orbit with perigee height within the effective atmosphere, each perigee passage sees eccentricity decrease and inclination increase. Thus, the orbit is seen to be contracting and becoming circular about the perigee height.

Possible co-planar soft maneuvers include aerobraking and rotation of the line of apsides. Multi-pass aerobraking (Walberg (1985)) uses the atmosphere to impart a velocity decrement with each pass. The result is a lowering of the apogee height with an eventual orbit circularization possible. The rotation of the line apsides is accomplished via either a drag-only (Vinh and Johannesen (1986)) or a combined drag and lift-assisted maneuver (Gur, et al. (1990)).

Single Pass AOTs ("Hard Maneuver"):

The "hard maneuver" entails forcing the vehicle to pull down deep into the atmosphere and performing the aeroassisted orbital transfer with a single pass. The main advantage of this scenario is the short time duration and the large magnitude of available aerodynamic forces to perform the maneuver. Its drawbacks include high heating rates and acceleration levels, and propellant requirements for deboost and reboost. The requirement for deboost and reboost and the associated propellant requirements severely limit the application of hard maneuvers to LightSat/TacSat stationkeeping AOTs, since these satellites carry such a limited amount of fuel. However, a hard maneuver may become feasible when the spacecraft is nearing the end of its orbital lifetime and is decaying into the atmosphere. The use of an aeroassisted maneuver may prolong orbital operations for several orbits. A political or military crisis may also necessitate a spacecraft performing a hard maneuver to position itself over a specific geographic region for a short period of time.

The hard maneuver plane change entails a deboost from orbit into the effective atmosphere. While in the atmosphere, the lift is modulated via bank angle and angle of attack to produce the desired plane change. The loss of energy during atmospheric pass is made up via a reboost impulse, and a reorbit impulse puts the vehicle into its final orbit.

The scenarios for co-planar AOTs using the hard maneuver follow those of the soft maneuver with the exception that they entail deeper penetration into the atmosphere and require only one pass.

2.1.2 Mission Requirements

LightSat/TacSat mission requirements that directly relate to the feasibility of application of AOTs are orbital geometry requirements (e.g., altitude, eccentricity, inclination, etc.) and orbit transfer or maneuver types.

Orbit Geometry:

Orbit geometry can be classified into size and shape of the orbit and orbit orientation. Size and shape of the orbit refer to parameters such as perigee altitude and eccentricity. Orientation refers to parameters such as inclination and perigee location.

For LightSat/TacSats, we will be dealing with satellites with perigee altitudes in the LEO range. Perigee altitude becomes an important factor in determining the feasibility of on-orbit soft maneuver AOTs. The perigee altitude must be low enough to ensure that atmospheric or aerodynamic forces are sufficient to alter the orbit in the desired manner. The range of feasibility for on-orbit soft maneuver AOTs becomes a function of what altitude is atmospheric density sufficient or in other terms, where does the effective atmosphere begin. If perigee altitude is lowered to within the effective atmosphere, there is concomitant detrimental effect on satellite on-orbit lifetimes. Satellite lifetime decreases with perigee altitude and eccentricity (Wertz (1985)). One way to offset this problem is to increase eccentricity while anchoring perigee location to within the effective atmosphere. Possible examples are highly eccentric orbits such as Molniya.

Inclination values for LightSat/TacSats may vary from sun synchronous orbits to Molniya orbits ($i = 63^\circ$) to other miscellaneous orbits. Sun synchronous orbits present the problem of maintaining inclination to meet the desired nodal regression rate. Molniya orbits have the advantage that the rate of rotation for the line of apsides is very nearly zero. Other orbital requirements for LightSat/TacSats may include localized global area coverage. This requirement would directly relate to a required inclination and a desired perigee location.

Maneuver Requirements:

Several maneuvers required of LightSat/TacSat can served by AOTs. As mentioned previously, inclination stationkeeping for sun synchronous satellites seems readily applicable, as well as for Molniya orbits. Another application of AOTs would be for anchoring perigee location or analogously compensating for the rotation of the line of apsides. Other orbital transfers also conducive to aeroassisted maneuvers include prolonging satellite lifetime once in a decaying orbit and redeployment of a satellite to a

strategic location. We present approximate analytical results for two of these maneuvers in the next section.

2.1.3 Satellite Parameters

Several satellite parameters directly affect overall feasibility of application of AOTs to LightSat/TacSats. Included in these are satellite mass, aerodynamic coefficients, satellite configuration, and propulsion capabilities.

Mass directly affects aerodynamic forces acting on a satellite travelling in the effective atmosphere in an inverse fashion. For a larger mass satellite, the effect of atmosphere, whether it be the drag force or a lifting force, is reduced. Larger mass acts beneficially to increase satellite lifetime. The range of satellite mass for this study is 25 to 250 kg (approximately 50 to 500 lbs.) and is inline with mass values for LightSat/TacSats.

Aerodynamic coefficients include the lift coefficient, C_l , and the drag coefficient, C_d . These parameters vary with satellite configuration, air flow, and altitude. A useful aerodynamic parameter is the maximum value of lift over drag or C_l/C_d attained by a vehicle. An aerodynamically efficient vehicle may have a C_l/C_d of greater than 1 and may exceed 2 for winged vehicles in a continuum flow. At orbital altitudes (heights greater than 200 km), a satellite encounters rarefied flow and values for C_d increase while C_l decreases. Typical values for C_d and C_l are around 2 and below 1, respectively (King-Hele (1987)). Nominal values of $C_d = 2$ and $C_l = 1$ will be used for our analysis.

Satellite configuration refers to the reference area S , which is the cross-sectional area perpendicular to the flow. For LightSat/TacSats, S could take values below 1 m^2 or as high as 6 m^2 when inflatable solar arrays are added. Our nominal value will be $S = 1 \text{ m}^2$.

Propulsion capabilities for LightSat/TacSats are very limited and are basically used for attitude control. We have assumed, therefore, no propulsion capabilities for our analysis of on-orbit soft maneuvers. The addition of propulsive forces allows for a greater amount of feasibility of hard maneuvers or deeper penetration into the atmosphere.

2.2 Analytical Results

We now present some analytical results pertaining to application of AOTs to LightSat/TacSats. We begin by exploring upper atmospheric density modeling and variation as it affects aeroassisted maneuvers. The equations of motions for endo- and exo-atmospheric flight are then presented. We then present approximate analytical results for

application of on-orbit soft maneuver AOTs to inclination stationkeeping and rotation of line of apsides.

2.2.1 Atmosphere Density Modeling & Variation

As stated previously, the soft maneuver can be performed on-orbit if the perigee altitude is within the effective atmosphere. To aid in the feasibility assessment of AOTs for LightSat/TacSats, we have reviewed the current research in atmospheric models and variations. Most of the results presented here are from King-Hele (1987) which contains an extensive treatment of the subject of atmospheric variations and effects on satellite orbits. Our research effort will focus on the atmospheric density levels at altitudes pertinent to the LightSat/TacSat community, since density relates directly to the aerodynamic forces of lift and drag via the following relationships:

$$\begin{aligned} L &= \frac{1}{2} C_l \rho S v^2 \\ D &= \frac{1}{2} C_d \rho S v^2 \end{aligned} \quad (2.1)$$

where C_l and C_d are the lift and drag coefficients, respectively, ρ is atmospheric density, S is the satellite reference area, and v is velocity. We first begin by looking at the density variation with altitude, then we discuss latitude variations, and then conclude with a brief discussion of other variations.

Variation with altitude:

Using the universal gas law and the hydrostatic equation, the variation of atmospheric density with altitude can be given by the following relationship (King-Hele (1987)):

$$\rho(h) = \rho_0 e^{\left(\frac{h - h_0}{H}\right)} \quad (2.2)$$

where h is altitude, ρ_0 is the density at the reference altitude h_0 , and H is the density scale height. The above equation assumes a symmetric spherical atmosphere and is seen to be accurate for altitudes up to 500 km.

Equation (2.2) shows an exponential behavior for density as a function of altitude. To gather further insight into actual values for density at orbital altitudes, figure 2-1 plots the mean value of density at altitudes from 100 km to 500 km using data from the COSPAR International Reference Atmosphere (COSPAR (1972)) as given in Wertz (1985). As shown in the figure, there is a sharp decrease in density over the range of increasing altitude. The decrease is especially noticeable, on the scale of three orders of magnitude,

when altitude increases from 100 km to 200 km. The levels of density shown are very low even for low orbital altitudes (i.e., 200 km) and we must therefore constrain ourselves to perigee heights below 200 km to ensure feasibility of on-orbit soft maneuver AOTs for LightSat/TacSats.

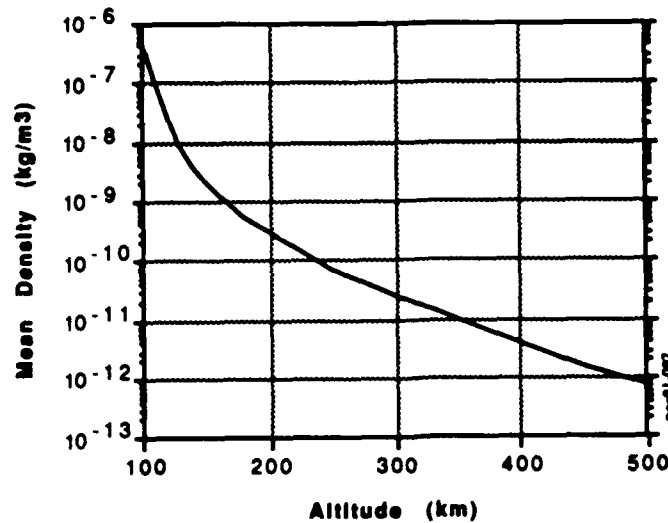


Figure 2-1: Upper Atmosphere Density Profile

Variation with latitude:

In the earlier expression for atmospheric density the assumption of a spherical earth was made. In reality the earth is an oblate spheroid and consequently the atmosphere is oblate. If we again assume that density varies exponentially with altitude at a given latitude, the expression for density becomes (King-Hele (1987)):

$$\rho(h) = \rho_{p0} e^{\left(\frac{r-\sigma}{H}\right)} \quad (2.3)$$

where r is the radius, H the scale height, ρ_{p0} the density at the initial perigee location and σ locates an oblate spheroid that passes through the initial perigee location of r_{p0} and given by:

$$\sigma = r_{p0} \frac{1 - \epsilon \sin^2 \phi}{1 - \epsilon \sin^2 \phi_{p0}} \quad (2.4)$$

with $\epsilon = 0.00335$ is the earth's ellipticity and ϕ represents latitude. For illustrative purposes, we plot in figure 2-2 the effect of an oblate atmosphere on density. The plot

shown is for a circular polar orbit of altitude of 200 km. Shown on the plot is the normalized density (with 1.0 being the initial density at the equator) as a function of latitude. We see a doubling of density when going from polar to equatorial latitudes. The overall effect of the oblate atmosphere depends on the perigee latitude and the rotation of perigee location.

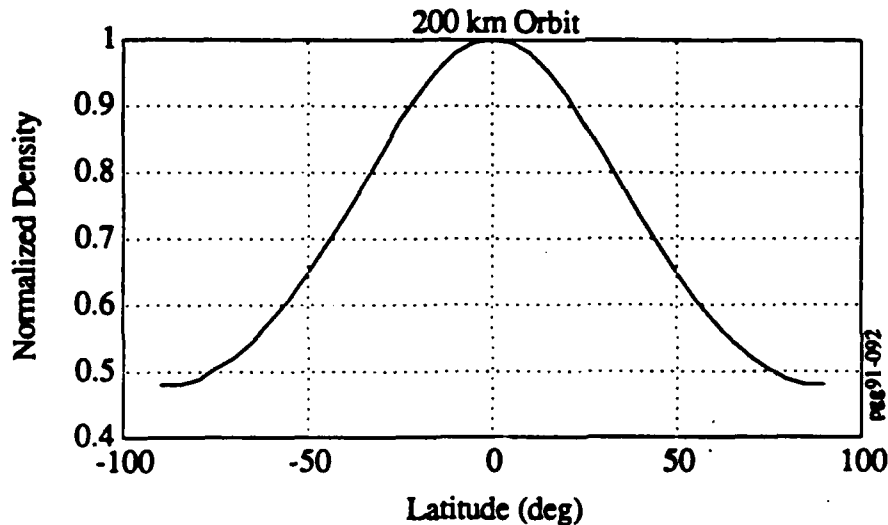


Figure 2-2: Density Variation with Latitude

Variations due to other effects:

Atmospheric density varies due to other effects, some of which are: day/night effects; solar activity; and seasonal effects. Day/night density variations are most evident between altitudes of 500-1000 km. Density during daylight may be as high as 5 times larger than nighttime. Solar activity effects are evident in the altitude range of 200-600 km and can cause an increase in density by an order of magnitude at an altitude as low as 400 km. Seasonal variations in density are evident at altitudes between 200 and 500 km. Density is seen to reach maxima near equinoxes and minima at the solstices with equinox density being about double the solstice density.

These variations and the latitude variation still do not compensate for the orders of magnitude decrease in density with increasing altitude, as shown in figure 2-1. For a feasible on-orbit AOT, perigee altitudes below 200 km maximum are required with the drawback that such perigee altitudes bring about short satellite lifetimes.

2.2.2 Problem Formulation

In this section we formulate the equations of motions for both endo- and exoatmospheric flight. The formulation follows that of Ikawa (1986) and has proven

suitable for as varied situations as an endo-atmospheric plane change maneuver, in-orbit flight, and cross-country flight of an airplane. The equations are specified for a rotating earth and assume an inverse square gravitational law. With the absence of aerodynamic and thrust forces, the equations reduce to Keplerian orbital mechanics, thus assuring continuity between orbital and atmospheric flight. Possible results available using the formulation include ground traces (latitude versus longitude), cross/down ranges, and relative and inertial velocities. We also derive an expression for satellite orbital lifetime which will be used in the feasibility assessment of on-orbit AOTs.

Equations of motion:

Restating the equations of motion from Ikawa (1986) allowing for no propulsive forces, we have:

$$\begin{aligned}
 \dot{r} &= v \sin \gamma \\
 \dot{\theta} &= \frac{v \cos \gamma \cos \psi}{r \cos \theta} \\
 \dot{\phi} &= \frac{v \cos \gamma \sin \psi}{r} \\
 \dot{v} &= \frac{D}{m} - g \sin \gamma + r \omega_E^2 F_1 \\
 \dot{\gamma} &= \frac{L \cos \mu}{m v} + \left(\frac{v}{r} - \frac{g}{v} \right) \cos \gamma + 2 v \omega_E C_2 + r \omega_E^2 F_2 \\
 \dot{\psi} &= \frac{L \sin \mu}{m v \cos \gamma} - \frac{v \cos \gamma \cos \psi \tan \phi}{r} - 2 v \omega_E C_3 - r \omega_E^2 F_3
 \end{aligned} \tag{2.5}$$

where

r	:	radius from the center of the Earth
θ	:	downrange angle along the reference plane
ϕ	:	crossrange angle normal to the reference plane
v	:	Earth relative velocity
γ	:	flight path angle (positive up in reference plane)
ψ	:	heading angle in reference plane
D, L	:	aerodynamic lift and drag as given by (2.1)
g	:	gravitational acceleration
μ	:	bank angle
ω_E	:	Earth's rotation rate
C_1, C_2	:	Coriolis acceleration coefficients
F_1, F_2, F_3	:	centrifugal acceleration coefficients

The reference plane is defined via the vehicle initial location in terms of inclination (i_0), nodal position (Ω_0), and downrange angle (θ_0). The vehicle's Earth-based latitude and longitude are calculated from the following:

$$\begin{aligned}\sin(\phi_{lat}) &= \sin(\phi) \cos(i_0) + \cos(\phi) \sin(\theta_0 + \theta) \sin(i_0) \\ \tan(\theta_{lon}) &= \frac{k_1 \sin(\Omega_0) + k_2 \cos(\Omega_0)}{k_1 \cos(\Omega_0) - k_2 \sin(\Omega_0)}\end{aligned}\quad (2.6)$$

with

$$\begin{aligned}k_1 &= \cos(\phi) \cos(\theta_0 + \theta) \\ k_2 &= \cos(\phi) \sin(\theta_0 + \theta) \cos(i_0) - \sin(\phi) \sin(i_0)\end{aligned}\quad (2.7)$$

The Earth-referenced latitude and longitude become equivalent to the crossrange and downrange angles, respectively, when i_0 , Ω_0 , and θ_0 are all zero.

Satellite lifetime:

An important quantity to consider in assessing the feasibility of AOTs for LightSat/TacSats is satellite orbital lifetime. Orbital lifetime is defined as the time from initial orbit injection to when the satellite orbit decays deep into the atmosphere and becomes inoperable. An approximate expression for satellite lifetime is found in Wertz (1985) and is given by:

$$L = (1.15185 \times 10^{-7}) \times N \times \left(\frac{r_E + h_p}{1 - e} \right)^2 \quad (2.8)$$

where L is lifetime in days, r_E the radius of the Earth, h_p the perigee height, e the eccentricity, and N the number of revolutions over the lifetime. Approximate values for N divided by the ballistic coefficient are plotted in Wertz (1985) for various perigee heights and various eccentricities. The ballistic coefficient is defined as:

$$B = \frac{m}{C_d S} \quad (2.9)$$

where m is satellite mass, S is the reference area, and C_d the drag coefficient, taken to be 2.0 for our analyses.

2.2.3 Inclination Stationkeeping

One possible scenario for the application of on-orbit aeroassisted orbital maneuvers to LightSat/TacSats is inclination stationkeeping. The scenario involves changing the satellite orbital plane by small amounts during each perigee pass to keep inclination within a desired range. For instance, a sun synchronous satellite requires a certain inclination value for a given altitude to remain sun synchronous. In this section we derive an approximate expression for plane change per orbital revolution.

The time rate of change of inclination can be expressed as Ikawa (1986):

$$\frac{di}{dt} = \frac{\cos(A_z) \cos(\phi_{lat})}{\sin(i)} \frac{L \sin(\mu)}{m v \cos(\gamma)} \quad (2.10)$$

where A_z is the initial heading azimuth of the inertial plane given by

$$\sin(A_z) = \frac{\cos(i)}{\cos(\phi_{lat})} \quad (2.11)$$

or analogously,

$$\cos(A_z) = \sqrt{\frac{\cos^2(\phi_{lat}) - \cos^2(i)}{\cos^2(\phi_{lat})}} \quad (2.12)$$

Using this expression in (2.10) results in

$$\frac{di}{dt} = \frac{\sqrt{\cos^2(\phi_{lat}) - \cos^2(i)}}{\sin(i)} \frac{L \sin(\mu)}{m v \cos(\gamma)} \quad (2.13)$$

This expression shows that an inclination change is most effective at low or equatorial latitudes. Letting latitude equal zero, we have

$$\frac{di}{dt} = \frac{L \sin(\mu)}{m v \cos(\gamma)} \quad (2.14)$$

It can be noticed that the inclination change is equal to the first term on the right-hand side for the heading equation in the equation of motions. If the Earth is assumed non-rotating and the vehicle is at low latitudes (i.e., $\tan(\phi) = 0$) then

$$\frac{di}{dt} = \frac{L \sin(\mu)}{m v \cos(\gamma)} = \frac{d\psi}{dt} \quad (2.15)$$

or the change inclination is equal to the heading change as in Hull, et al. (1985).

We now make several more assumptions to simplify the expression for inclination change. We assume that perigee occurs at equatorial latitudes such that the last expression for inclination is a good approximation. Assuming the maneuver occurs around perigee makes the flight path angle roughly zero and replacing the lift force with the expression for L in (2.1), the expression for inclination change now becomes:

$$\frac{di}{dt} = \frac{C_l \rho S v \sin(\mu)}{2m} \quad (2.16)$$

Inclination change is maximized for \sin of bank angle = 1 or bank angle = 90° . Inserting this value for μ and assuming the right-hand of the equation remains constant over the perigee pass the expression for inclination change per revolution for a unit mass satellite becomes:

$$\Delta i = \frac{1}{2} C_l \rho S v \Delta t \quad (2.17)$$

where Δt is the time spent within the perigee pass. Two of the parameters affecting the inclination change cannot be altered: the atmospheric density is a function of altitude and the satellite velocity is determined by the orbit. We are therefore left with three parameters that can be altered to increase inclination change: the aerodynamic lift coefficient; the reference area S ; and the time elapsed during perigee crossing. Increasing the lift coefficient is hampered by the rarefied flow encountered at orbital altitudes and by an associated increase in aerodynamic drag which reduces orbital lifetime. An increase in reference area also increases drag and reduces lifetime. The time elapsed during the perigee pass is constrained by the height of the effective atmosphere.

We now consider an orbit with the a perigee height at 200 km and apogee height of 1600 km. The aeroassisted maneuver is assumed to begin at an altitude of 250 km and continues through the perigee height of 200 km until altitude reaches 250 km again. The time elapsed Δt of this perigee pass if calculated to be 677.7 s using Keplerian orbital mechanics. The velocity is assumed to be the velocity at perigee or 8.15 km/s. The atmospheric density is taken as an average value between heights 200 and 250 km from the density table in Wertz (1985) and is $1.76e-10$ kg/m³. The resulting inclination change per revolution for a unit kg satellite is now:

$$\Delta i = 0.02785 C_l S \quad (2.18)$$

A 25 kg (= 50 lbs) satellite with a 1 m² surface area with C_D of 1 would attain 0.00111 deg/rev of plane change or 0.51° change over the orbital lifetime of 33 days as calculated using (2.8). A 250 kg (= 500 lbs) satellite with a 1 m² surface area with C_D of 1 would attain 0.000111 deg/rev of plane change or, again, 51° change over the orbital lifetime of 330 days. We would expect better performance by solving the actual optimal control problem and integrating the equations of motion over the orbital revolutions. In section 2.3, we perform several trade studies by varying parameters associated with the inclination stationkeeping maneuver and analyze the resulting effects.

2.2.4 Rotation of Line of Apsides

Another possible scenario for the application of aeroassisted orbital maneuvers to LightSat/TacSats is rotation of the line of apsides. This scenario is a transfer between coplanar elliptical orbits with eccentricity and semi-major axis fixed. This maneuver may be required to compensate for the rotation of the argument of perigee due to the Earth's oblateness. The AOT is accomplished by modulation of lift and drag during each perigee pass to garner the required apsidal rotation. In this section we derive an approximate expression for apsidal rotation per orbital revolution.

If we concern ourselves with planar motion, no constraints or boundary conditions imposed on longitude, a non-rotating Earth, and zero bank angle, the equations of motion (2.5) can be written as:

$$\begin{aligned}\dot{r} &= v \sin \gamma \\ \dot{v} &= \frac{D}{m} - g \sin \gamma \\ \dot{\gamma} &= \frac{L}{m v} + \left(\frac{v}{r} \frac{g}{v} \right) \cos \gamma\end{aligned}\tag{2.19}$$

The time rate of change of the line of apsides per unit mass as given in Gur, et al. (1990) is:

$$\frac{d\omega}{dt} = - \frac{(2 D \sin v + L (2 e + \frac{r}{a}) \cos v)}{e v}\tag{2.20}$$

where D and L are the lift and drag forces, respectively, v is true anomaly, r is radius, a is the semi-major axis, v is velocity, and e is eccentricity. Through the perigee pass the following assumptions can be made:

$$\begin{aligned}v &= 0 \\ \gamma &= 0 \\ v &= v_p\end{aligned}\tag{2.21}$$

where v_p is the perigee velocity. The equations for apsidal rotation rate and velocity now become:

$$\begin{aligned}\frac{d\omega}{dt} &= -\frac{L(2e + \frac{r}{a})}{e m v} \\ \frac{dv}{dt} &= -\frac{D}{m}\end{aligned}\quad (2.22)$$

Substitution of r with r_p , where the radius at perigee is given by:

$$r_p = a(1 - e) \quad (2.23)$$

results in a new expression for $d\omega/dt$.

$$\frac{d\omega}{dt} = -\frac{L(1 + e)}{e m v} \quad (2.24)$$

Dividing the expression for dv/dt by $d\omega/dt$ gives the velocity depletion rate per change in apsidal rotation or using (2.1), (2.22) and (2.24),

$$\frac{dv}{d\omega} = \frac{e v C_d}{(1 + e) C_l} \quad (2.25)$$

Inspection of (2.25) shows that for constant v , the velocity loss per rotation angle is minimized when C_d/C_l is minimum, or conversely, when C_l/C_d is maximum. Using this result and rewriting (2.24) in its final form, we have:

$$|\Delta\omega| = \frac{\rho C_l S v (1+e) \Delta t}{2 m} \quad (2.26)$$

where the absolute value takes into account the fact that lift can be negative or positive and where Δt is the time spent within the perigee pass.

Considering again an orbit with the a perigee height at 200 km and apogee height of 1600 km. The apsidal rotation maneuver is assumed to begin at an altitude of 250 km and continues through the perigee height of 200 km until altitude reaches 250 km again. The time elapsed Δt of this perigee pass as calculated before is 677.7 s, the velocity at perigee is 8.15 km/s, eccentricity is 0.1, and atmospheric density is constant at $1.76e-10$ kg/m³. The resulting apsidal rotation per revolution for a unit kg satellite is:

$$\Delta\omega = 0.0305 C_l S \quad (2.27)$$

A 25 kg (\approx 50 lbs) satellite with a 1 m^2 surface area with C_L of 1 would attain 0.00122 deg/rev of apsidal rotation or 0.56° change over the orbital lifetime of 33 days. A 250 kg (\approx 500 lbs) satellite with a 1 m^2 surface area with C_L of 1 would attain 0.000122 deg/rev of apsidal rotation or, again, 56° change over the orbital lifetime of 330 days. Once again, these are conservative estimates and we would expect better performance by solving the actual optimal control problem and integrating the equations of motion over the orbital revolutions. In the following section, we perform several trade studies by varying parameters associated with the apsidal rotation maneuver and analyze the resulting effects.

2.3 Trade Studies

In this section we document the performance of trade studies to determine the overall design drivers. The analytical results of the on-orbit stationkeeping maneuvers of the previous section are used to analyze both vehicle configuration and overall mission requirements. Specific items to be considered include: perigee height; orbital eccentricity; satellite reference area; satellite mass; and aerodynamic coefficients. The nominal set of these parameters defined for these studies are listed below in table 2-1. The two assumptions made are that the perigee location is at low latitudes and the aeroassisted maneuver begins and end at a height of 50 km above perigee.

Table 2-1: Nominal Parameter Set for Trade Studies

<u>Parameters:</u>	<u>Value:</u>
Perigee Height :	150 km
Eccentricity:	0.1
Satellite Mass	25 kg
Aerodynamic Coefficients	$C_L = 1, C_D = 2$

2.3.1 Variation of Perigee Height

A greater amount of plane change and apsidal rotation per revolution can be attained if perigee height is decreased resulting in an increase in atmospheric density. Using the two assumptions stated above and the nominal parameter set of table 2-1, we vary perigee height from 100 to 200 km. The results are shown in figures 2-3 and 2.4 for the plane change maneuver and apsidal rotation, respectively. Inspection of both figures shows orders of magnitude increase in maneuver capability per revolution when going from 200 km to a 100 km perigee height. Such an increase in maneuver capability is offset by the low orbital lifetimes at such altitudes, especially for low eccentricities. For the nominal

parameters of an 150 km perigee and $e = 0.1$, orbital lifetime is on the order of only 10 days.

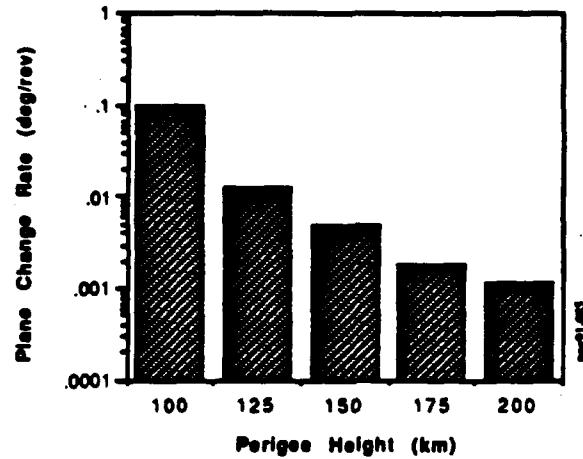


Figure 2-3: Effect of Perigee Height Variation on Inclination

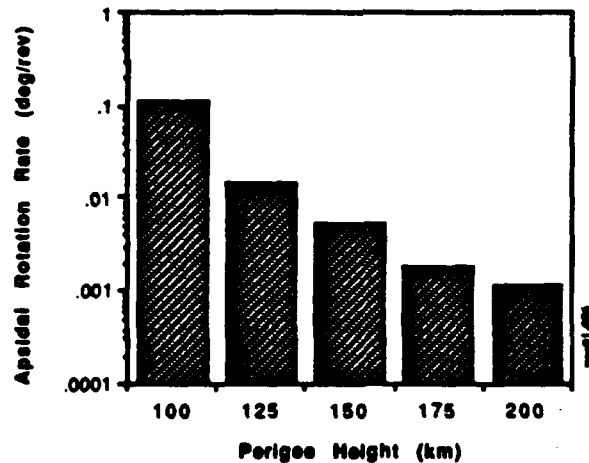


Figure 2-4: Effect of Perigee Height Variation on Apsidal Rotation

2.3.2 Variation of Eccentricity

To garner the advantageous effect eccentricity has on orbital lifetime, we plot in figures 2-5 and 2.6 the inclination change and the apsidal rotation per revolution, respectively, and the associated lifetime for a range of eccentricities from 0.1 to 0.6. Figure 2-5 shows the amount of plane change per revolution decreasing with increasing eccentricity while lifetime increases. What is noticeable is that the decrease in plane change is by a factor of two over the eccentricity range. However, lifetime increases an order of magnitude from about 10

days to almost one year for $e = 0.6$. Figure 2-6 shows the amount of apsidal rotation per revolution decreasing initially with increasing eccentricity, as with plane change, but then flattening out at higher values of e while lifetime increases. The flattening out effect at higher e is due to the $(1+e)$ term in the numerator of (2.26). The decrease in apsidal rotation is by a factor of less than two over the eccentricity range with again lifetime increasing from about 10 days to almost one year for $e = 0.6$.

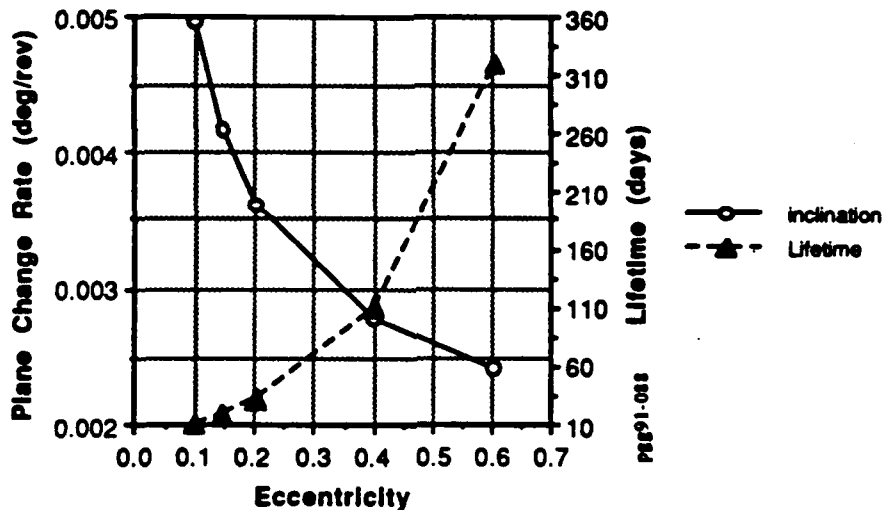


Figure 2-5: Effect of Eccentricity Variation on Inclination and Orbital Lifetime

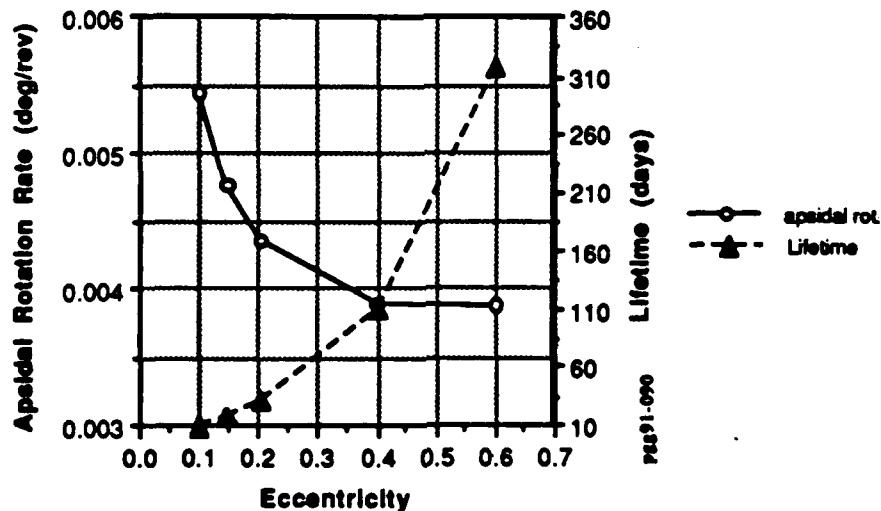


Figure 2-6: Effect of Eccentricity Variation on Apsidal Rotation and Orbital Lifetime

More information is obtainable by plotting the total amount of plane change and apsidal rotation incurred over the orbital lifetime as shown in figures 2.7 and 2.8. We see that the higher eccentricity orbit not only has a longer lifetime, as was shown in figures 2-5 and 2.6, but over the total lifetime achieved a greater amount of plane change and apsidal rotation. The results shown in these figures lead us to conclude that higher eccentric orbits at relatively low perigee heights are feasible for performing inclination and perigee location stationkeeping.

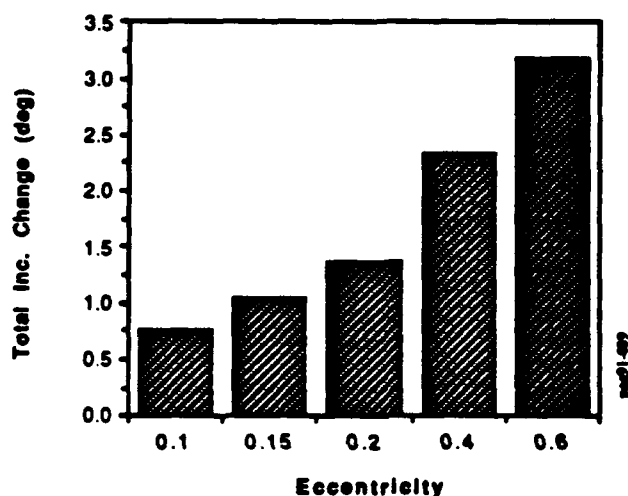


Figure 2-7: Total Inclination Change Over Orbital Lifetime for Varying Eccentricity

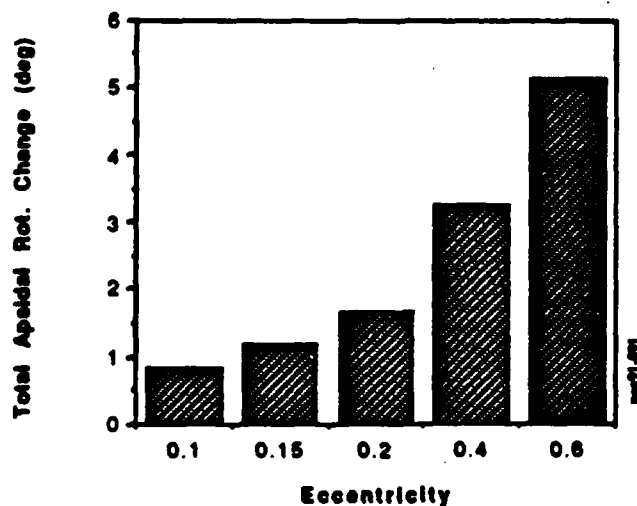


Figure 2-8: Total Apsidal Rotation Change Over Orbital Lifetime for Varying Eccentricity

2.3.3 Variation of Reference Area

An increase in satellite reference area, S , has a beneficial effect on plane change and apsidal rotation, as per (2.17) and (2.26), while orbital lifetime is decreased, as given by (2.8). Both of these effects are linear in S . To gather more insight, we vary S from $.25 \text{ m}^2$ to 6 m^2 and use the other nominal parameter values from table 2-1 to compute amount of plane change and apsidal rotation per revolution. The values that S may take are based on current LightSat/TacSat configurations and envisioned future configurations (e.g., deployable solar arrays). Figures 2-9 and 2-10 plot the results for varying S and at different eccentricities. The figures show the beneficial effect of increased S has on the maneuvers with a maximum effectiveness occurring at $S = 6 \text{ m}^2$ with $e = 0.1$.

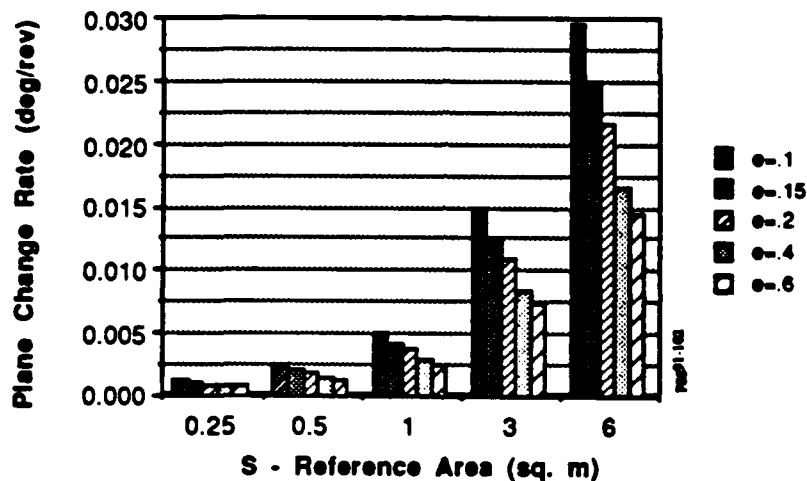


Figure 2-9: Effect of Reference Area Variation on Inclination

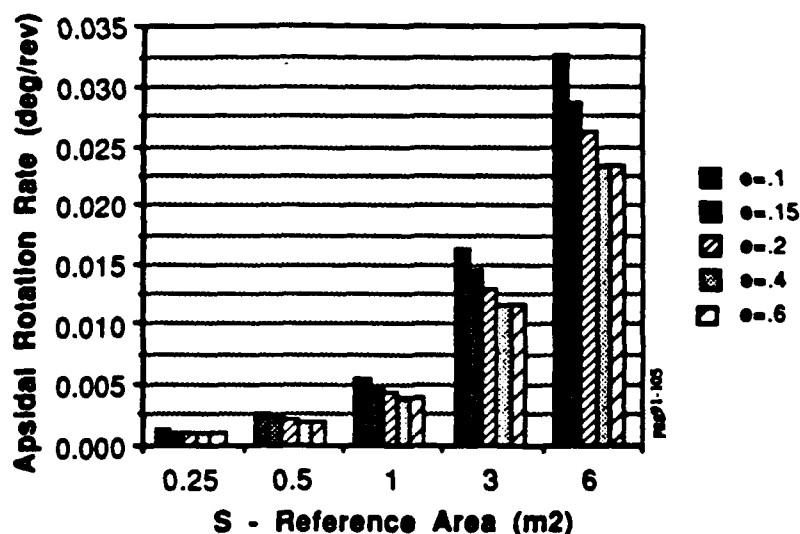


Figure 2-10: Effect of Reference Area Variation on Apsidal Rotation

The beneficial effect of increased S has on plane change and apsidal rotation is offset by the decrease in orbital lifetime. Figure 2-11 plots orbital lifetime versus S for the range of eccentricities considered. As shown, there is over an order of magnitude decrease in lifetime over the range of S . The $S = 6 \text{ m}^2$ $e = .1$ case, which produced the largest maneuvers is seen to have an orbital lifetime of only about two days. Thus, we see a counter-balancing effect between maneuver effectiveness and decreased lifetime. This is pointed out in figures 2-12 and 2-13 where we plot both total inclination change and apsidal rotation, respectively, over satellite lifetime and lifetime itself for an eccentricity of 0.6. The figures show that total inclination change and apsidal rotation are constant over S , while lifetime decreases. That is, more orbital change is accomplished faster with larger values of S but with total change over lifetime equal for all S . We conclude that a desired value for S is one in which the requirements of orbital maneuvering and satellite lifetime are both considered. We may envision deployment of articulated booms or arrays to increase S to generate more maneuverability in an emergency satellite deployment situation, or conversely stowage of arrays or booms to decrease drag and keep satellite at an operational altitude.

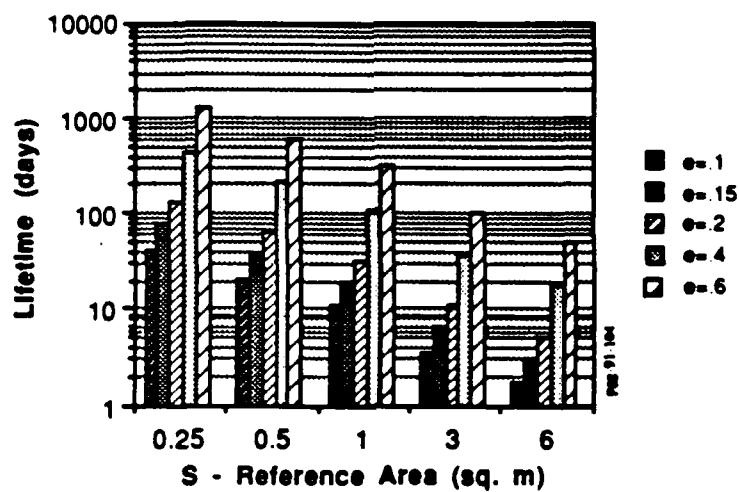
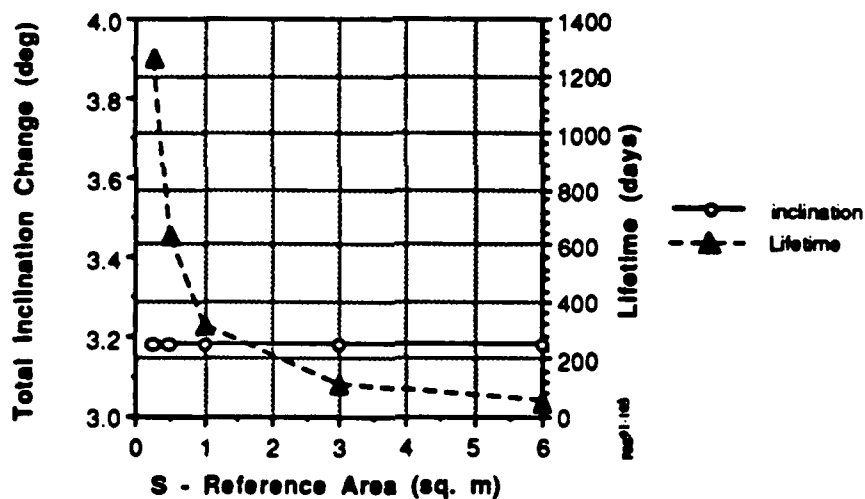


Figure 2-11: Effect of Reference Area Variation on Orbital Lifetime

Figure 2-12: Effect of Reference Area Variation on Total Inclination Change and Orbital Lifetime ($c=0.6$)

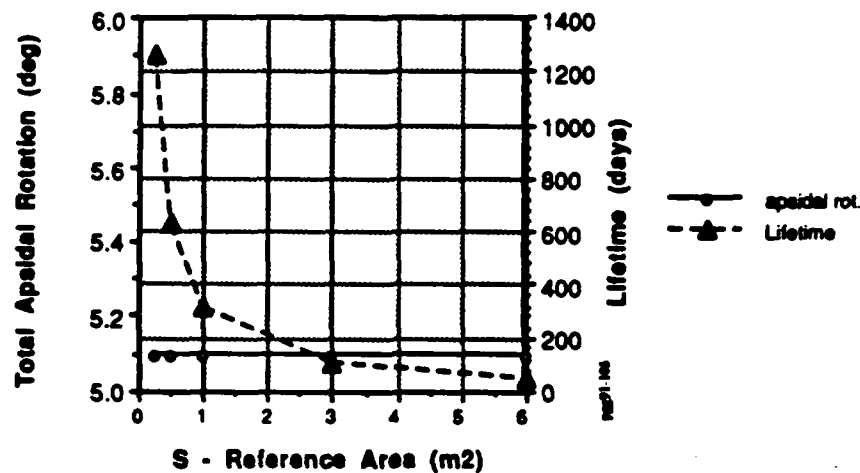


Figure 2-13: Effect of Reference Area Variation on Total Apsidal Rotation and Orbital Lifetime ($e = 0.6$)

2.3.4 Variation of Satellite Mass

The range of satellite mass considered for this study, as mentioned previously, is 25 to 250 kg. Mass decreases plane change and apsidal rotation as shown by (2.17) and (2.26). However, mass has a beneficial effect on orbital lifetime by increasing the ballistic coefficient which in turn increases the number of orbital revolutions in a lifetime. Figure 2-14 plots plane change per revolution for the range of mass considered at different eccentricities for the nominal parameter set, whereas figure 2-15 does the same for apsidal rotation. As shown, we see the linear decrease in maneuver amount with increasing mass and again the decrease with higher eccentricity. Lower mass, while producing a greater plane change and rotation per revolution, comes with lower lifetime cost as can be seen by considering the $e = 0.6$ case. Figure 2-16 plots orbital lifetime and total achievable inclination change, whereas figure 2-17 does the same for apsidal rotation. Figures 2-16 and 2-17 show that total inclination change and apsidal rotation are constant over mass, while lifetime increases. That is, a greater amount of maneuver is accomplished faster with smaller masses but with total orbital change over lifetime equal for all masses.

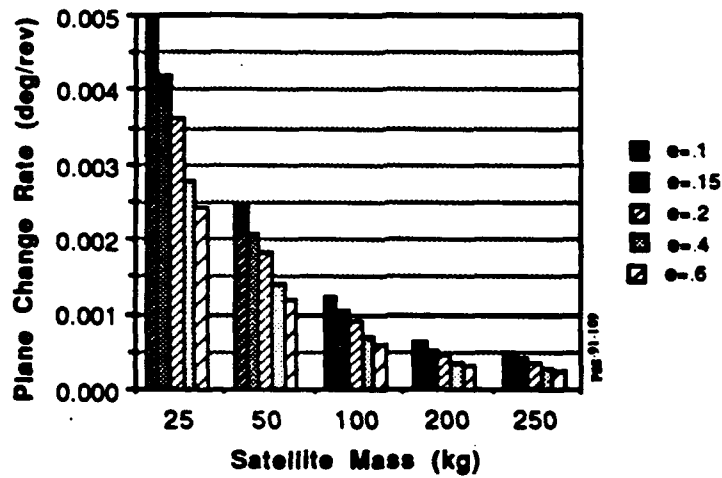


Figure 2-14: Effect of Satellite Mass Variation on Inclination

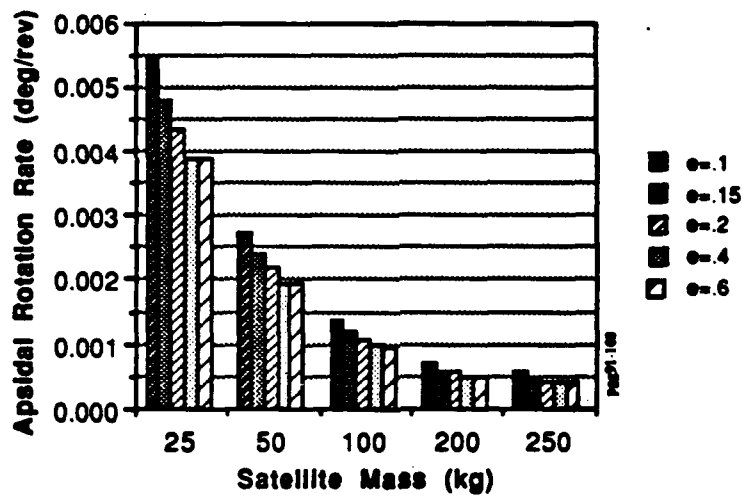


Figure 2-15: Effect of Satellite Mass Variation on Apsidal Rotation

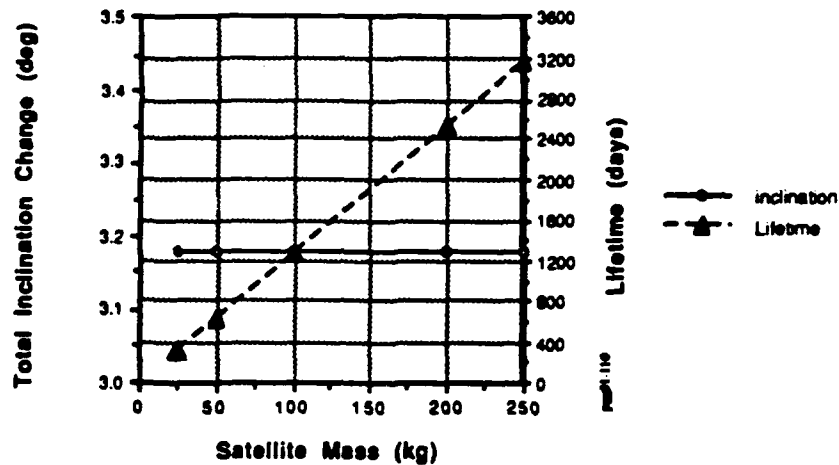


Figure 2-16: Effect of Satellite Mass Variation on Total Inclination Change and Orbital Lifetime ($e=0.6$)

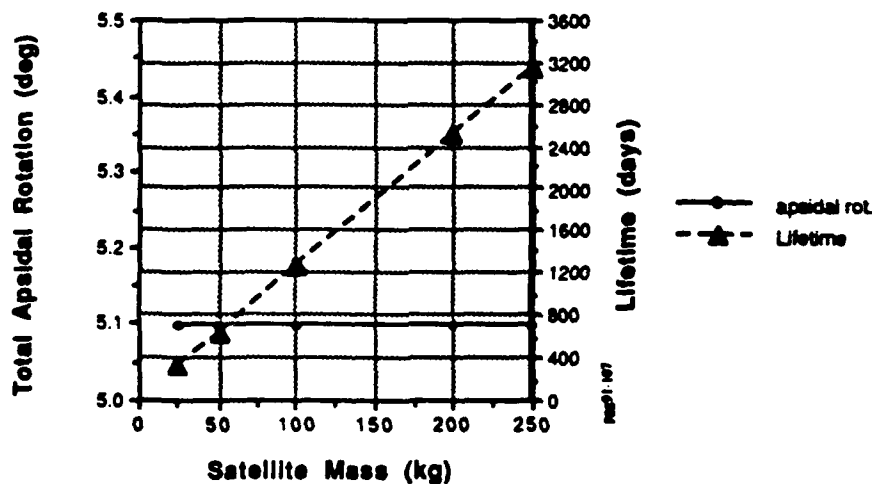


Figure 2-17: Effect of Satellite Mass Variation on Total Apsidal Rotation and Orbital Lifetime ($e=0.6$)

2.3.5 Variation of Aerodynamic Coefficients

The lift and drag coefficients (C_l , C_d) provide a measure of aerodynamic efficiency of a vehicle and determine how much lift and drag are generated at a given velocity and density. In our simplified analysis for inclination and perigee location stationkeeping, a higher lift coefficient relates directly to a greater plane change (2.17) and apsidal rotation (2.26). The drag coefficient plays an important factor in orbital lifetime. A satellite with a larger C_d decays more rapidly. In a continuum flow regime, C_l may be increased and C_d decreased by altering the shape of the vehicle. However, most satellites encounter rarefied flow in which the molecular mean free path exceeds a typical linear dimension of the body.

Rarefied flow produces a drastic increase in drag with an accompanied reduction in lift. At altitudes of 200 km and above, C_d may be as high as 2.2 with C_l below .1. For lower altitudes, an approximate formula for C_d is obtained in King-Hele (1987) and is given by:

$$C_d \approx 1.94 \exp(-1/K) + 1.01 \exp(-K/10) \quad (2.28)$$

where K is the Knudsen number, i.e., the ratio of mean free path to satellite length. King-Hele (1987) also presents a plot relating K with altitude and satellite length. K is found to be about 0.5 for a 1 m² long satellite at an altitude of 100 km. Evaluating (2.28) with this value of K leads to C_d of 1.25 at 100 km. If we do an exponential curve fit to the stated values at 100 and 200 km for C_d , the following variation with altitude is obtained:

$$C_d(h) = 0.71023 \exp(-5.653 \times 10^{-3}h) \quad (2.29)$$

Further assuming that the lift-over-drag ratio (L/D) decreases from 1 at $h = 100$ km to 0.1 at $h = 200$ km (typical values found in the literature), we obtain the following lift coefficient variation with altitude:

$$C_l(h) = 7.1023 \exp(-1.737 \times 10^{-2}h) \quad (2.30)$$

The resulting exponential curve fits for C_l and C_d are shown in figure 2-18.

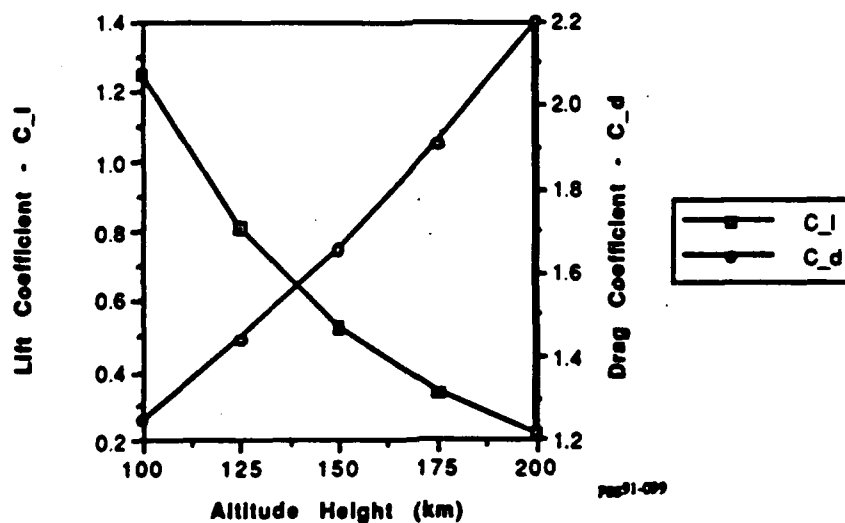


Figure 2-18: Variation of Aerodynamic Coefficients with Altitude

Figure 2-19 plots plane change rate for a range of perigee heights between 100 and 200 km. Analogously, figure 2-20 plots apsidal rotation for the same perigee range. Both

figures use the lift coefficient variation of (2.30) and the nominal parameters stated previously. The figures show the orders of magnitude decrease in plane change and apsidal rotation per revolution with increasing altitude due to density and lift coefficient reduction. The results are comparable with those presented on perigee height variation (figures 2-3 and 2-4) with superimposition of the effect of aerodynamic coefficient variation. These results further the necessity for performing maneuvers at lower altitudes.

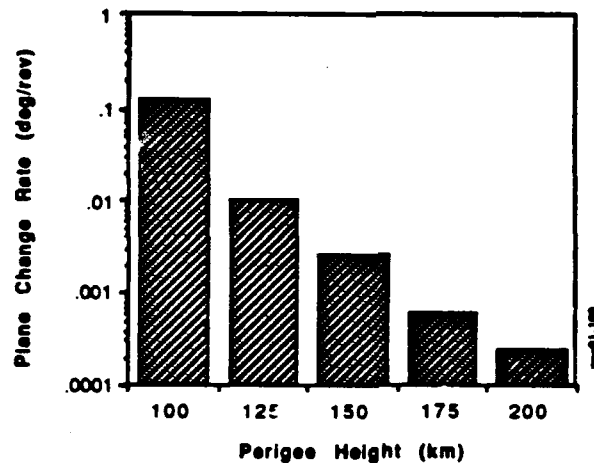


Figure 2-19: Effect of C_L Variation on Inclination

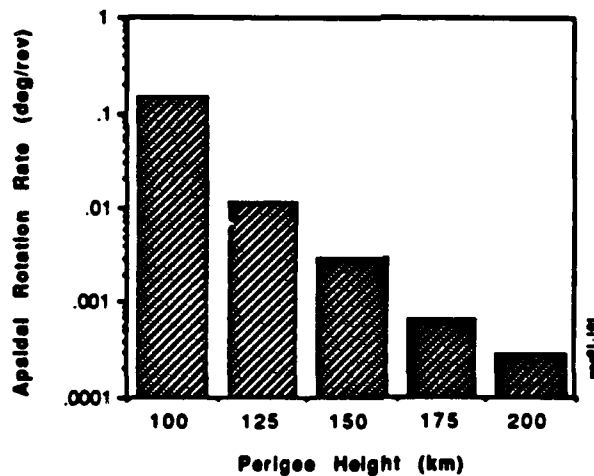


Figure 2-20: Effect of C_L Variation on Apsidal Rotation

2.3.6 Trade Studies Overall Results

Several design drivers have been identified from our analysis work. For the two maneuvers considered and from investigating the upper atmosphere density variations,

perigee height determines where the "effective" atmosphere is located or where aeroassisted maneuvers become feasible. Our analysis shows that a perigee height to about as high as 200 km is where feasibility of AOTs exist. Beyond 200 km the atmospheric forces become almost negligible. Other identified design drivers include perigee location, satellite orbital lifetime, and initial orbit eccentricity. Perigee location becomes important for inclination changes since these are more effective at equatorial latitudes. Satellite orbital lifetime and eccentricity are directly related since higher eccentricities prolong orbital lifetime, whereas a decrease in perigee location decreases lifetime. Thus, as was shown in our analysis, lowering perigee altitude to take advantage of greater aerodynamic force while increasing eccentricity to offset the decrease in lifetime, makes AOTs more feasible. Other possible design drivers to be considered include variation in satellite reference area and varying aerodynamic coefficients.

2.4 Feasibility Assessment of AOTs

In this section we discuss the overall feasibility of applying aeroassisted orbital transfers to LightSat/TacSats. We begin by discussing applicable scenarios and then focus on aspects that relate directly to feasibility including control actuation, propulsion technologies, and possible interaction of AOTs with satellite subsystems.

2.4.1 Applicable AOT Scenarios

Two AOT scenarios have demonstrated feasibility based on the results of the previous section. These are the inclination change and apsidal rotation on-orbit or soft maneuvers. A total lifetime inclination change of over 3 degrees or a total lifetime apsidal rotation of greater than 5 degrees was demonstrated for a 25 kg satellite in an orbit with a perigee height of 150 km and eccentricity of 0.6. These results will increase if the Earth oblate atmosphere is considered and once the optimal solution is obtained. Further increases in maneuverability are possible at lower perigee heights with more aerodynamic vehicles (e.g., a maneuver in Vinh and Ma (1990a,b) accomplished 20° of plane change). Possible application of these types of maneuvers may be inclination stationkeeping for a satellite with near-equatorial perigee location or compensating for rotating argument of perigee for satellites in near Molniya orbits (i.e., $i = 63.4$). For example, if we consider a 12 hour Molniya orbit with a perigee altitude of 150 km and satellite parameters as used in section 2.3, the approximate amount of $\Delta\omega$ achieved using an AOT per orbital revolution is 4×10^{-3} degrees from (2.26) or 8×10^{-3} degrees per day. The argument of perigee rotation rate per day due to oblateness is approximately (Wertz and Larson (1991)):

$$\Delta\omega = 1.03237 \times 10^{14} a^{-3.5} (4 - 5 \sin^2(i))(1 - e^2)^{-2} \quad (2.31)$$

If we compare the achievable apsidal rotation rate with the rotation due to oblateness at near Molniya inclinations, we see that perigee location stationkeeping could be accomplished via AOTs for inclinations $\pm 0.5^\circ$ from the nominal zero apsidal rotation inclination of 63.4° . AOTs could therefore be used to compensate for these off-nominal orbital conditions that may arise from orbital injection errors.

Other possible feasible AOT scenarios include orbit circularization, emergency satellite redeployment, and controlled satellite deorbiting. Aeroassisted circularization of an orbit may be accomplished via the multi-pass soft maneuver. Through each perigee pass energy is lost with the resulting apogee height being decreased. The use of hard maneuvers, i.e., maneuvers involving a propulsive deboost burn to enter the atmosphere, may also be feasible for future LightSat/TacSats that employ more propulsive capabilities. The literature is replete with examples demonstrating the fuel savings encountered using the synergetic plane change or the aerobraking maneuver (see the bibliography in Appendix A). Another interesting application of AOTs may be the controlled deorbit of a satellite. As a satellite's orbital lifetime nears the end, its orbit finally circularizes and then it begins to spiral earth-bound. AOTs can be envisaged for several scenarios during deorbit: to prolong orbital lifetime by a few revolutions; relocating the satellite to deorbit over a strategic geographic area; and controlled deorbit to allow for recovery (e.g., the Navy's Parafoil Orbital Recovery Program (PORT)).

2.4.2 Feasibility Aspects

Controller Actuation:

Aeroassisted maneuvers require active control surfaces to control the lift and drag forces. For the inclination stationkeeping maneuver discussed in section 2.2.3, the amount of plane change is related to the bank angle of the spacecraft. Thus to accomplish this maneuver, the spacecraft must be rotated about its roll axis. The apsidal rotation stationkeeping maneuver of section 2.2.4 only requires in-plane maneuvering via modulation of lift and drag forces. This is accomplished by varying the satellite's angle of attack or pitch attitude. The question arises as to how to perform these control actuations. Several options are available to choose from including passive and active attitude control methods. Limited passive actuation methods possible for LEO satellites include the use of gravity-gradient torques for slow rate pitch control or slewing the solar arrays to provide pitch and roll reorientation in the presence of large aerodynamic forces. More involved

attitude maneuvers require the use of active actuation methods. Reaction wheels and thrusters are typical active actuators. Reaction wheels provide a cost and weight effective method for lower rate ($< 0.5^\circ$ slewing maneuvers), whereas thrusters can perform higher rate maneuvers (i.e., satellite banking for plane change). In the next section we address issues related to current and envision propulsion technologies that relate to the feasibility of AOTs for LightSat/TacSats.

Propulsion Technologies:

The use of propulsive techniques furthers the feasibility of AOTs for LightSat/TacSats. Increased propulsive capabilities may allow for the use of hard maneuvers (i.e., a deeper penetration into the atmosphere) to perform larger more involved orbital transfers. However, propulsive capability comes with a concomitant increase in satellite weight, cost and complexity. Currently some LightSat/TacSats use cold gas propulsion systems. Cold gas provides a simple, reliable, very low cost system. Its disadvantages are heavy weight and low performance. Liquid propellant systems offer more performance but with higher complexity and cost. Current electric propulsion systems provide high performance with low weight and system complexity but are limited by low thrust capability and high power requirements. Future propulsion systems such as laser-based schemes may offer better performance at lower costs and weights, and thus making AOTs that much more feasible for LightSat/TacSats.

AOT Subsystem Interaction:

An important aspect to consider for AOT feasibility is the interaction the maneuver may have with onboard subsystems. Some relevant issues are listed below for each of the main satellite subsystems.

GN&C: How will the AOT affect payload/satellite pointing requirements? What further requirements does the AOT impose on attitude control?

Communication: What are the uplink/downlink and telemetry requirements to perform an AOT?

Power: How does an AOT maneuver impinge satellite power generation, storage, distribution, and regulation and control? What the power requirements of an AOT?

Thermal: What are the requirements that the AOT imposes on the thermal control subsystem as far as temperature limits and survivability?

Data Management: Is there any dedicated onboard software required to perform the AOT? What are the required data storage and data rates?

Structure/Mechanism: Does the AOT require any unique structure/mechanisms? What is its overall effect on overall satellite/payload structural integrity?

3. Neural Network Approach to AOT Guidance

In this chapter we describe a neural network approach to LightSat/TacSat AOT guidance. Section 3.1 discusses the objectives of using a neural net approach to develop closed-loop guidance laws. Section 3.2 then presents an overview of the backpropagation neural network paradigm used to develop the neural net guidance laws described in this report. Next, in section 3.3 we detail the development of closed-loop neural net guidance laws for a specific AOT maneuver. In particular, we present the generation of an optimal trajectory database for this maneuver, the neural net training databases derived from the trajectory database, the neural net architectures developed to model the optimal solution, and the training, open-loop, and closed-loop performance of the neural guidance laws. Section 3.4 concludes with a feasibility assessment of on-line neural network implementation of an atmospheric trajectory/guidance schemes.

3.1 Neural Net Guidance Objectives

Trajectory/guidance optimization for an AOTs requires the solution of a two-point boundary value problem with state and control constraints. Variational calculus yields a set of nonlinear differential equations for the state and co-state vectors as necessary conditions of optimality with split boundary values and en route constraints. The numerical solution of the necessary conditions is not a trivial task using current numerical techniques due to the stability characteristics of the co-state equations, and the sensitivity to parameter (atmospheric density, aerodynamic coefficients) changes (Halyo and Taylor (1989)). While off-line solutions are feasible using efficient numerical algorithms such as multiple shooting, on-line numerical solutions remain unattainable. Here, we assume that a suitable database of optimum guidance trajectories is available since significant recent research has focused on obtaining better numerical algorithms for obtaining these optimum trajectories.

Our approach is the neural network modelling of such an optimum trajectory/guidance database in order to obtain a closed-loop guidance law. Neural networks represent a nonalgorithmic class of information processing for using massively parallel distributed processing architectures. A neural net structure is a network of processing elements connected through information links. Each processing element is a multi-input/single-output dynamic system described by a first-order nonlinear differential equation.

Artificial neural networks produce a nearest-neighbor classifier. Conceptually, artificial networks are applicable to AOT guidance problems for learning the spatiotemporal attributes of optimum guidance/trajectories for a given class of problems. Once the neural

net is trained with an optimum trajectory/guidance database, it can then be used on-line to generate optimum guidance commands adapting to the uncertainties of the AOT operations. Such a neural network based guidance approach would be the nonalgorithmic counterpart to finding closed-loop guidance laws using algorithmic methods such as singular perturbation theory or energy state approximations. Given the emergence of recent fast, relatively inexpensive VLSI designs for realizing neural network structures, the implementation of neural net based space vehicle guidance systems will soon become feasible.

3.2 Backpropagation Neural Networks

The neural guidance architectures described in this report are developed using the backpropagation neural network paradigm. Backpropagation neural networks are well suited for problems where a given input vector is to be mapped into a desired output vector (Hecht-Nielsen (1991)). For the optimum guidance problem, the network maps current measurements, boundary conditions, and en route constraints into guidance commands. We present a brief overview of backpropagation neural networks below; detailed presentations of the backpropagation algorithm are contained in Rumelhart and McClelland (1988) and Hecht-Nielsen (1991). A description of the backpropagation neural network simulator used to develop the neural guidance networks described in this report can be found in Baffes (1989).

A backpropagation neural network consists of hierarchically connected *layers* of processing units or *nodes*. The nodes of one layer are fully or partially connected to the nodes of the following layer by *paths* which have an associated *weight*. Backpropagation networks typically have an input layer, an output layer, and one or more hidden layers which separate the input and output layers. Figure 3-1 illustrates a generic backpropagation network. The number of nodes in the input layer (l) and the number of nodes in the output layer (n) are dictated by the given problem. The number of hidden layers and the number of nodes in the hidden layers are determined by the network developer.

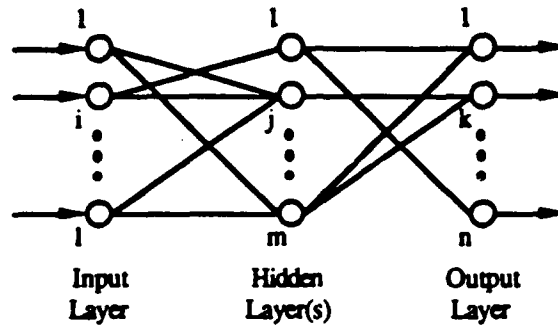


Figure 3-1: Backpropagation Neural Network

In a back propagation network, each node in the hidden and output layers outputs a weighted summation of its inputs plus a bias after a pass through a threshold nonlinearity (figure 3-2). Each node in the input layer outputs its input value unchanged. Here, we use the *sigmoid activation function* for the threshold nonlinearity since the desired output ranges are continuous.

Specifically, the j 'th node output is give by the following equation:

$$o_j = \frac{1}{1 + e^{-(\sum_i w_{ji} o_i + \theta_j)}} \quad (3.1)$$

where o_i is the output of the i 'th node, w_{ji} is the weight associated with the link from the i 'th node to j 'th node, and θ_j is a bias weight associated with a link from an imaginary node with output 1 to the j 'th node. Note that the output (o_j) in (3.1) will always be between 0 and 1.

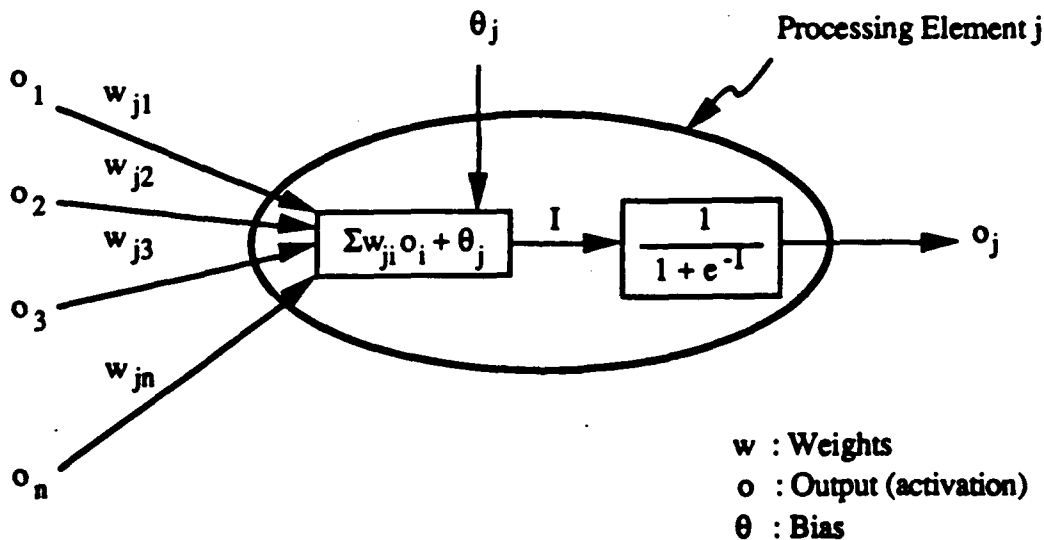


Figure 3-2: Back Propagation Processing Element

Backpropagation neural networks are *trained* to generate the desired output vector for a given input vector. Training involves repeatedly presenting the network with training data. Training data consists of several sets of input vectors and the corresponding output vectors (usually called IO pairs). After each IO pair is presented to the network, the error between the desired output vector and the actual output vector is calculated and the weights of the network are adjusted to minimize the error. (A detailed description of the generalized delta rule which governs the weight adjustments is given in Baffes (1989)). This "learning" process continues until the difference between the actual output and the desired output is acceptable.

3.3 LightSat/TacSat Neural Net Guidance Development

Here, we detail the development of neural net architectures for modelling a class of LightSat/TacSat AOT guidance/trajectory optimization solutions. Our design methodology is illustrated in figure 3-3. The initial step in the design process is the creation of an optimum trajectory database, assuming that optimum trajectories can be computed off-line using established numerical optimization techniques. This database contains the optimum trajectories between a set of initial and final states for a selected guidance scenario. The class of trajectories used here are for an aeroassisted multi-pass plane change maneuver and described in section 3.3.1.

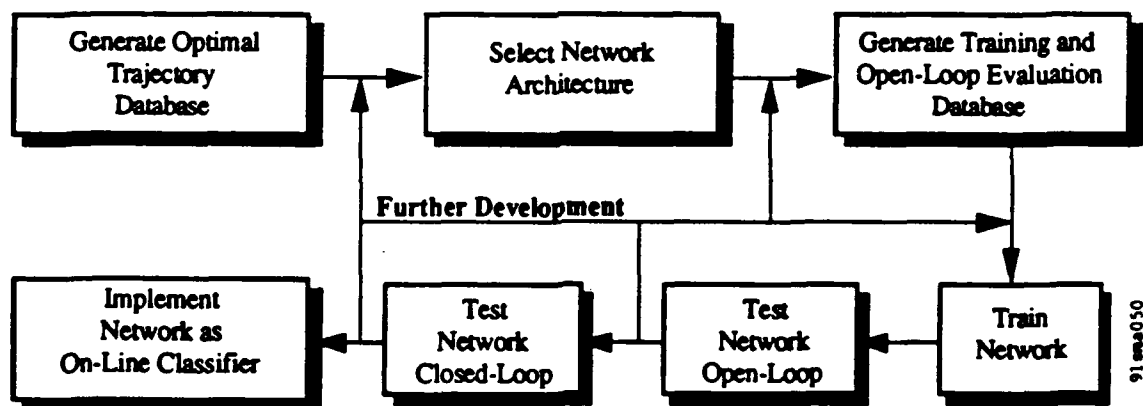


Figure 3-3: Neural Net Guidance Design Methodology

The next step in the design methodology is to select a neural net architecture for modelling the optimum trajectory/guidance database. Selecting a network architecture requires determining the network's inputs and outputs and defining its interconnect structure. In determining the network's inputs/outputs, we use our a priori knowledge about the optimal guidance solution. In the AOT guidance problem, the necessary conditions of optimality are readily available even though the closed-form analytic solution

cannot usually be obtained without approximations. Once the inputs/outputs are selected, network interconnect structures are defined. For the multi-pass plane change maneuver described here, we develop two sets of inputs/outputs, and seven network interconnect structures.

For a given neural network architecture, the network parameters are trained off-line using a training database which is a transformed subset of the optimal trajectory database. Training continues until an acceptable level of error is reached between the desired outputs and network outputs. At this point the neural net has "learned" the functional relationships between the inputs and the desired guidance commands. The network parameters are then frozen and the performance of the trained neural net is evaluated in both an open- and closed-loop fashion. If performance is deemed satisfactory, then the neural network can be implemented as an on-line classifier, otherwise further development is required.

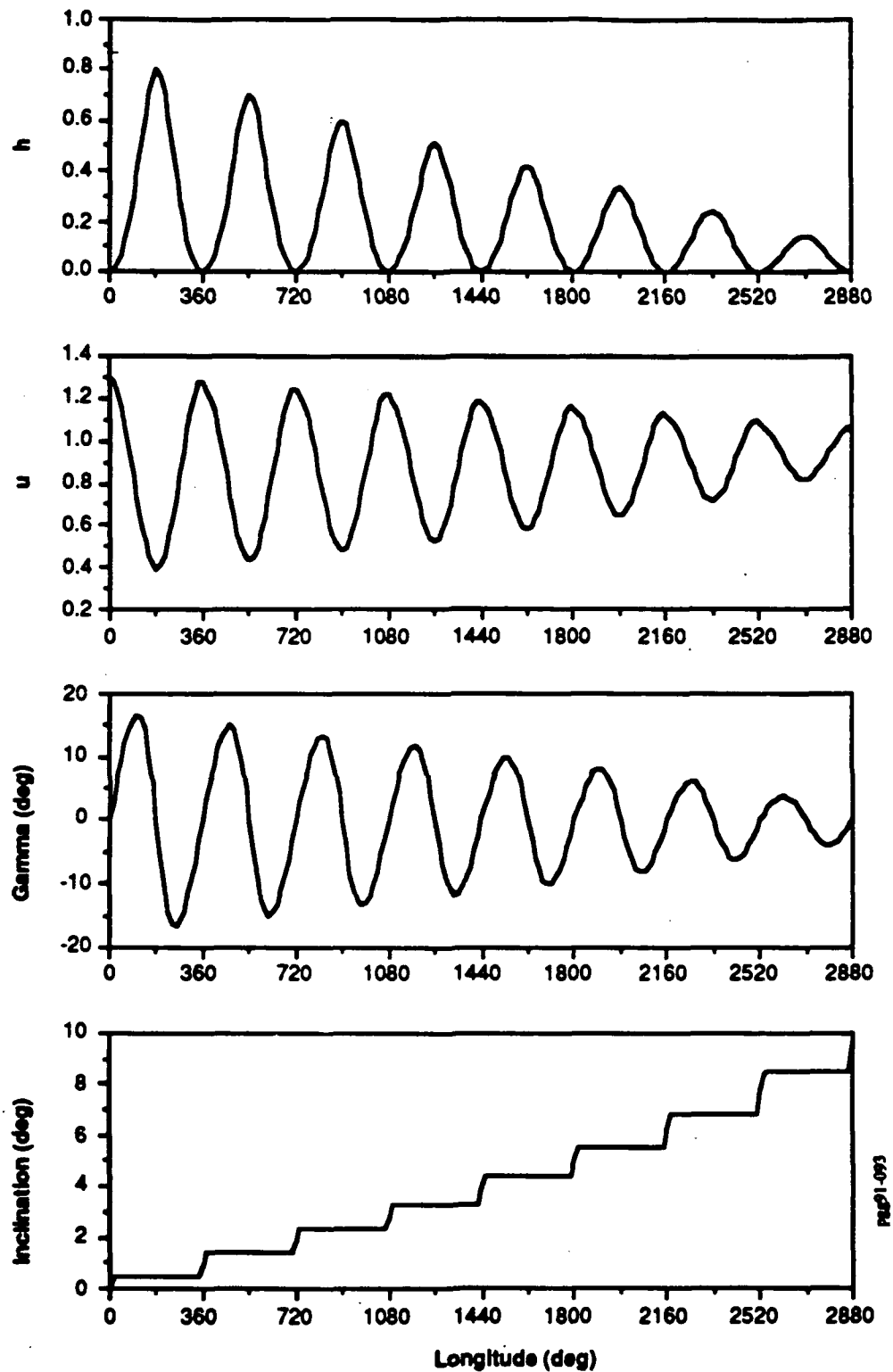
3.3.1 Neural Net Guidance Trajectory Database

To provide a trajectory database for the neural network guidance training and evaluation, we consider the plane change soft maneuver documented in Vinh and Ma (1990a) and Vinh and Ma (1990b). The maneuver is comparable to the plane change scenario envisaged for LightSat/TacSats and discussed in the previous chapter. The specific scenario involves a moderately aerodynamically efficient vehicle (maximum $C_y/C_d = 1.5$) at an initially eccentric zero inclination orbit with a perigee height approximately in the 100 km range flying in a spherical non-rotating atmosphere. The problem of maximizing plane change is formulated using dimensionless variables and the necessary conditions for optimality are posed. An assumption that aerodynamic forces are negligible when compared to gravity allows for optimal lateral and vertical lift coefficients (or analogously, the normalized lift coefficient and bank angle) to be obtained in an explicit form.

A simulation has been developed to propagate the state histories and the approximate optimal controls. The controls are the vertical and lateral lift coefficients denoted by C and S , respectively. The six dimensionless states are $[h \ \theta \ \phi \ \psi \ u \ \gamma]^T$ where, as before in (2.5), θ is longitude, ϕ is latitude, ψ is heading, and γ is flight path angle. The other dimensionless states h and u represent altitude and speed, respectively, and are given by:

$$\begin{aligned} h &= \frac{r - r_0}{r_0} \\ u &= \frac{v^2}{v_{\text{circ}}^2} \end{aligned} \tag{3.2}$$

where r_0 is the initial radius and v_{circ} is the circular orbital speed at the perigee altitude. Trajectories were generated for three different initial values for u_0 : $u_0 = 1.3$, 1.45 , and 1.6 . Trajectories conclude when $h = 0$ and $u = 1$ (i.e., the orbit has been circularized). State and control trajectories are shown in figures 3-4 and 3-5 for $u_0 = 1.3$, figures 3-6 and 3-7 for $u_0 = 1.45$, and figures 3-8 and 3-9 for the $u_0 = 1.6$, respectively. Several aspects become apparent from these figures: 1) the control trajectories are sinusoidal with longitude; 2) flight path angle, altitude (h), and velocity (u) tend to circularization; 3) there is stepwise increase inclination with each revolution; and 4) the three trajectories exhibit similar trends with the larger u_0 cases attaining more plain change due to their higher initial eccentricities.

Figure 3-4: State Trajectories ($u_0 = 1.3$)

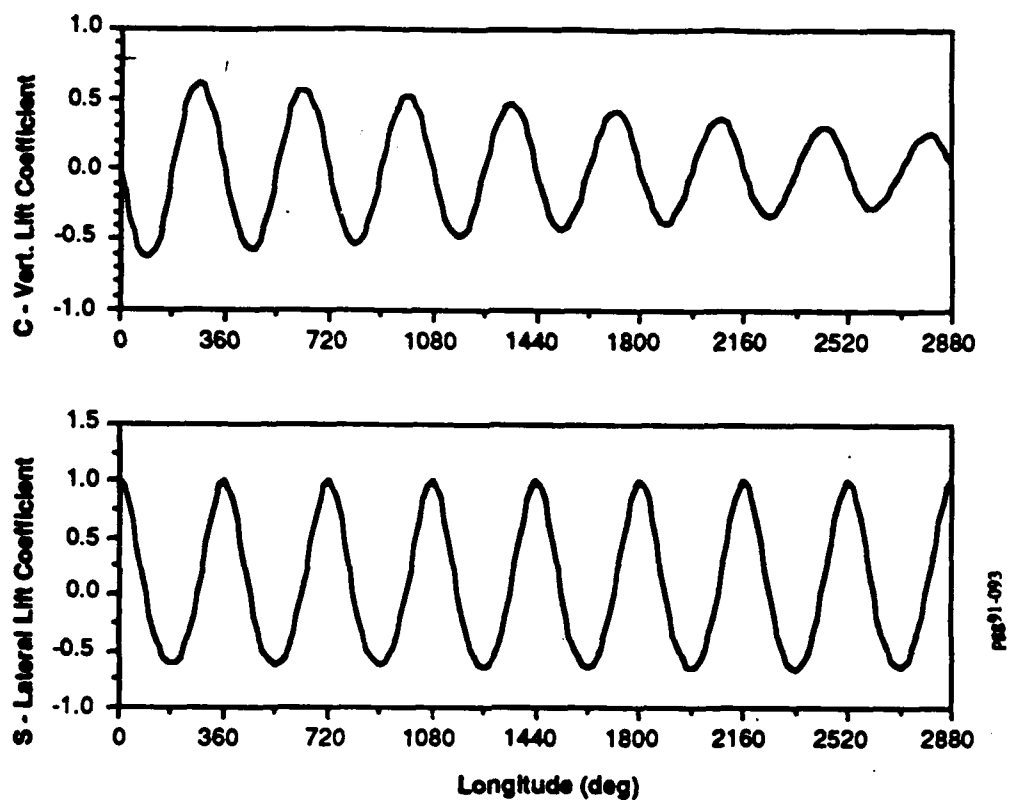


Figure 3-5: Control Trajectories ($u_0 = 1.3$)

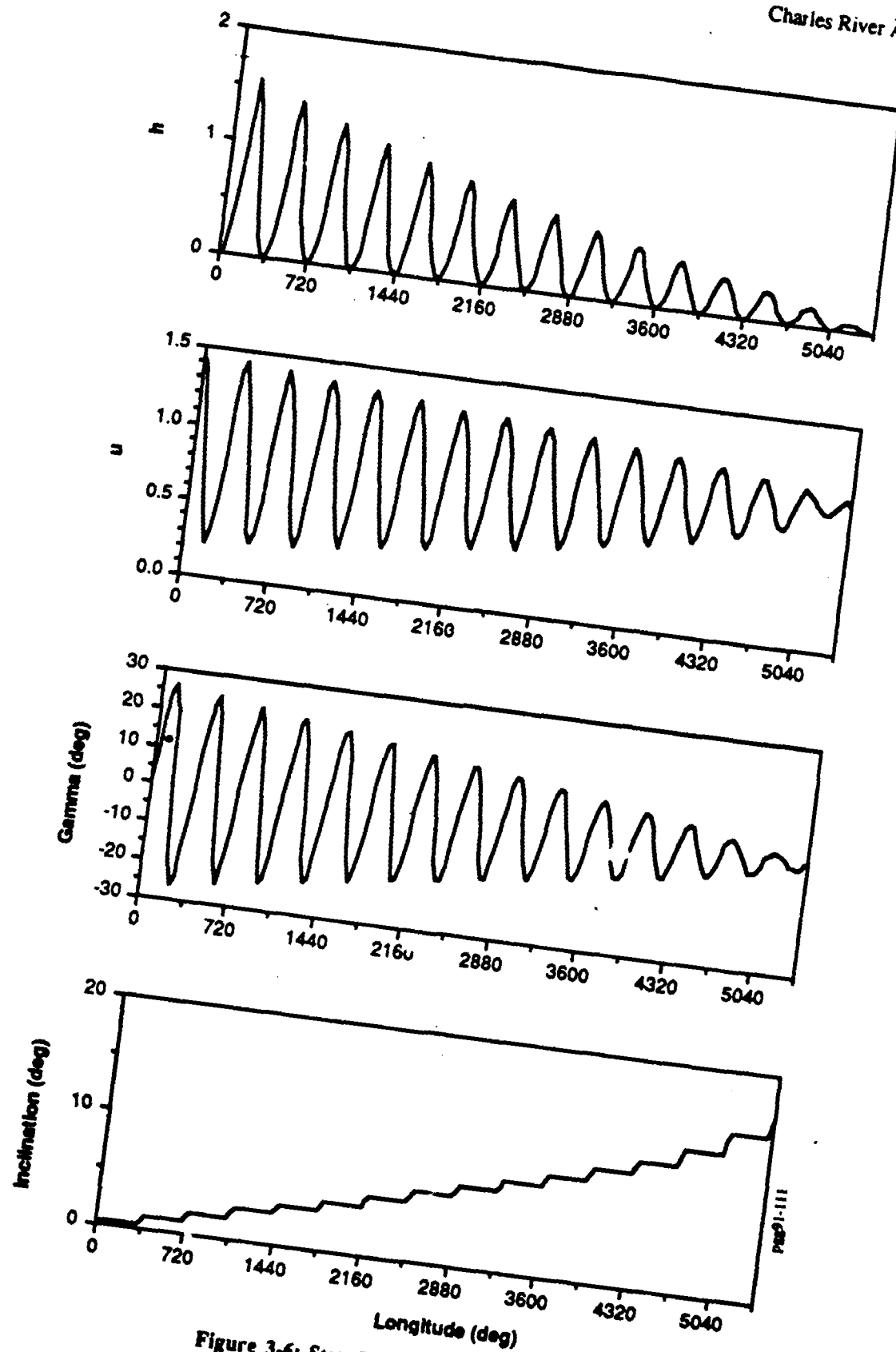


Figure 3-6: State Trajectories ($u_0 = 1.45$)

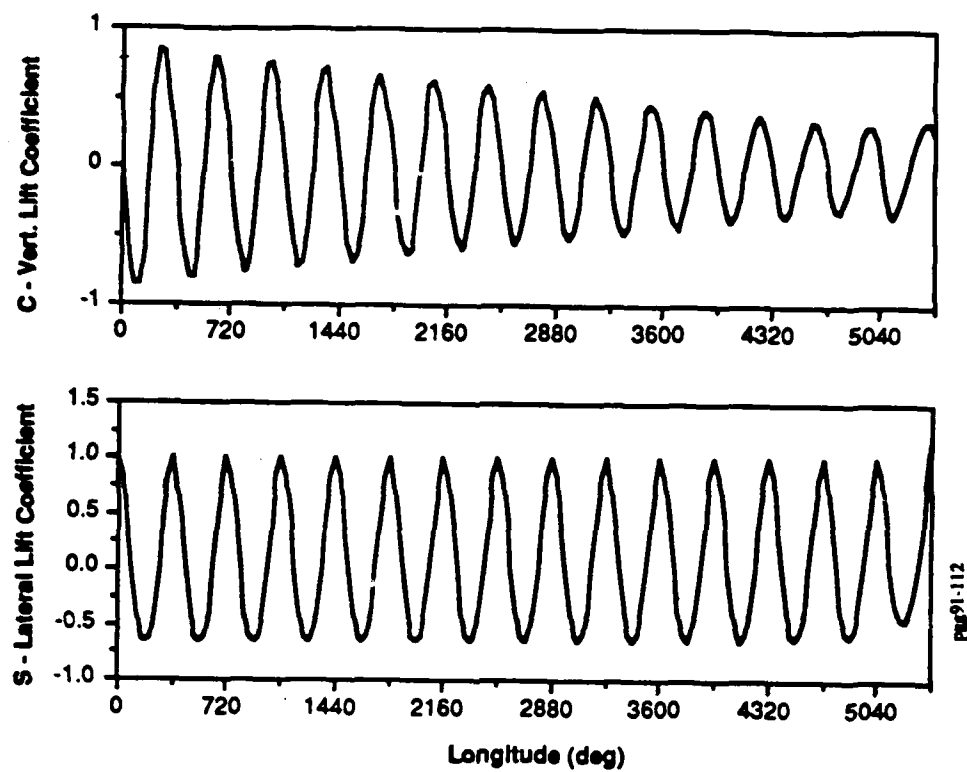
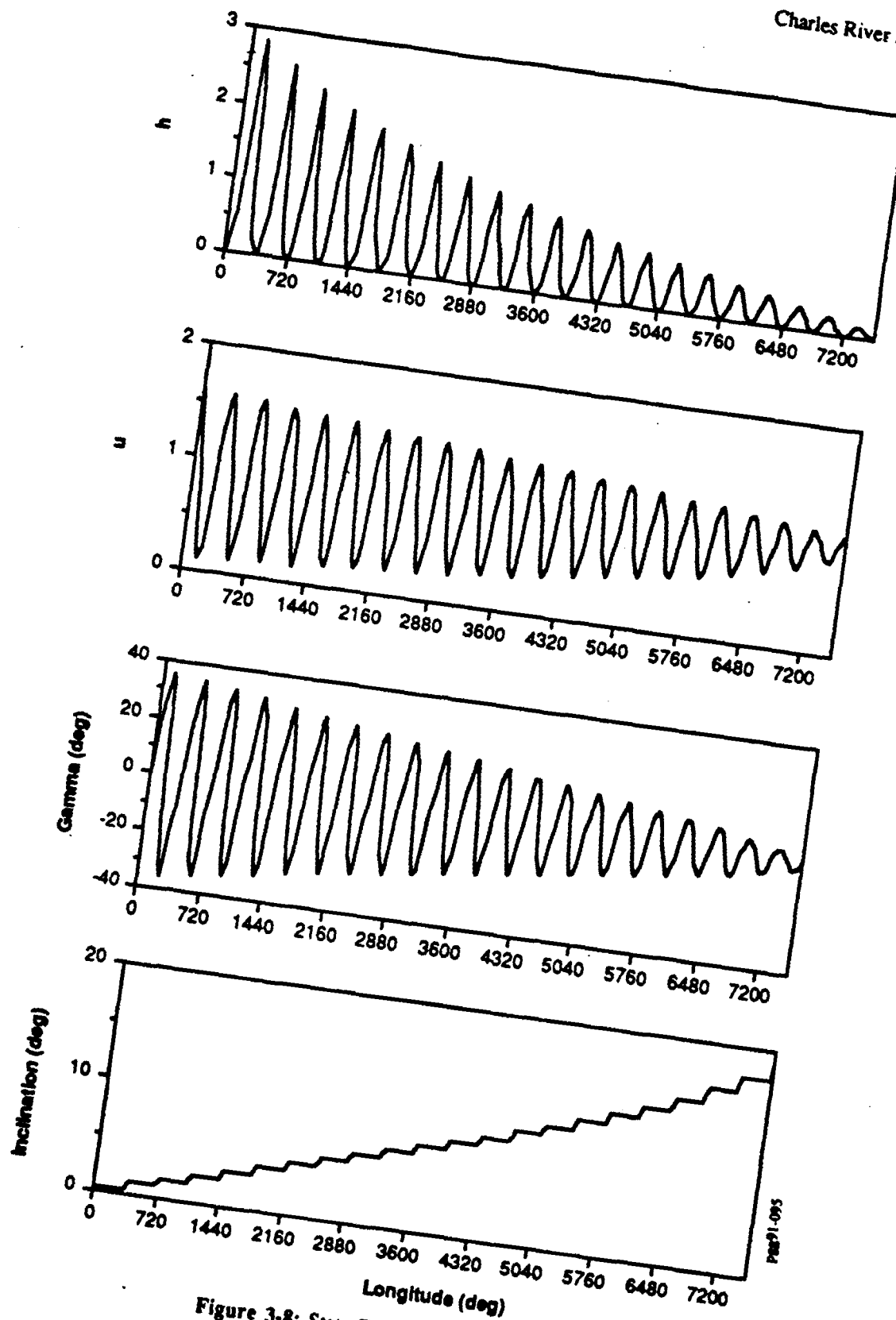
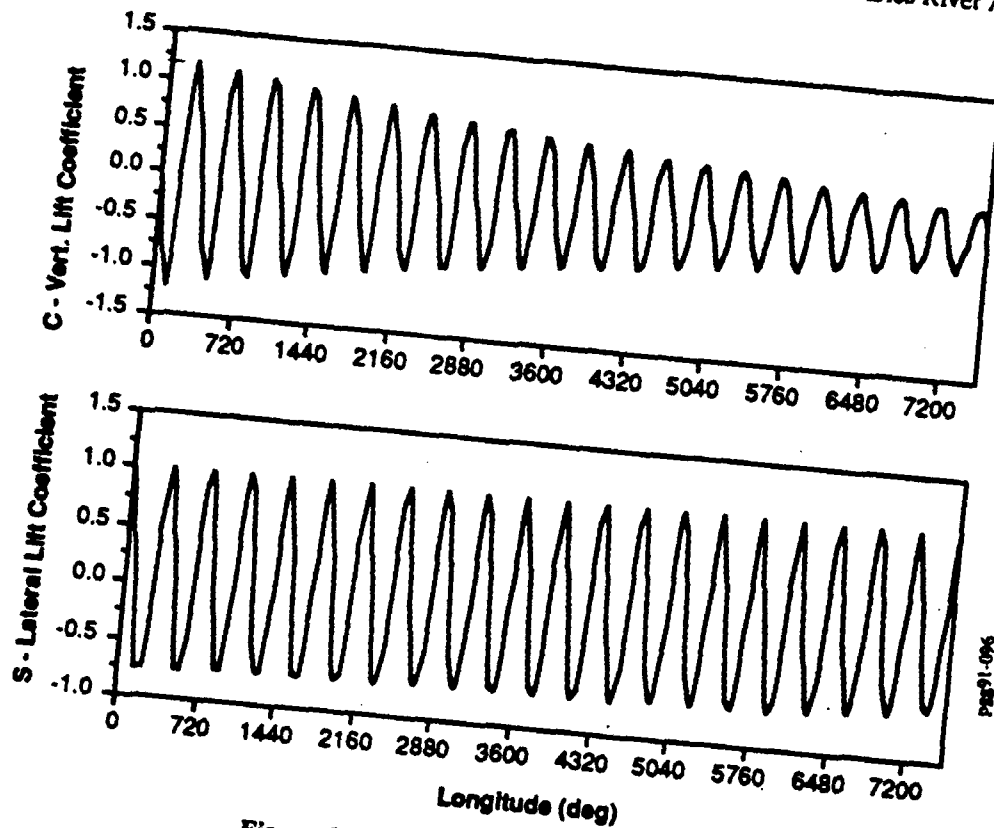


Figure 3-7: Control Trajectories ($u_0 = 1.45$)

Figure 3-8: State Trajectories ($u_0 = 1.6$)

Figure 3-9: Control Trajectories ($u_0 = 1.6$)

3.3.2 Neural Net Guidance Architecture Selection

The first step in the neural net modelling of the optimum trajectory database is to determine the inputs and outputs of the network. Since the vertical and lateral lift coefficients C and S are the controls for the problem described in section 3.3.1, they should clearly be the network outputs. In selecting the network inputs, we use our a priori knowledge about the optimal guidance solution. Following this approach, we derive two different sets of inputs: I/O Set 1 and I/O Set 2. Both I/O sets have the same number of inputs so that we can compare their training, open-loop, and closed-loop performances on identical network interconnect structures.

I/O Set 1:

The inputs of I/O Set 1 are derived from the dimensionless states $[h \ \theta \ \phi \ \psi \ u \ \gamma]^T$ and from the form of the control trajectories. As mentioned in section 3.3.1, the control trajectories are sinusoidal with the independent variable longitude (θ). Incorporating this information into the inputs improves the learning process and network performance. Therefore, $\cos\theta$, and $\sin\theta$ are used instead of longitude as inputs. Also note that the amplitude of C decays with longitude (figures 3-5, 3-7, and 3-9), therefore $e^{-c\theta}$ is used as

an input. The decay constant (c) is set to 0.035. This slows rate of exponential decay to more closely match the decay in C for all three sets of trajectories, $u_0 = 1.3, 1.45$, and 1.6 . Latitude (ϕ) and heading (ψ) can be represented by a single variable, the inclination angle (I). Selecting I as an input will simplify the network without losing the trajectory information associated with ϕ and ψ . The remaining three states, altitude (h), velocity (u), and flight path angle (γ), are used as inputs directly. The initial value of velocity (u_0) is also an input to the network since it contains information that distinguishes between the three trajectories. Figure 3-10 illustrates I/O Set 1 for a single hidden layer network.

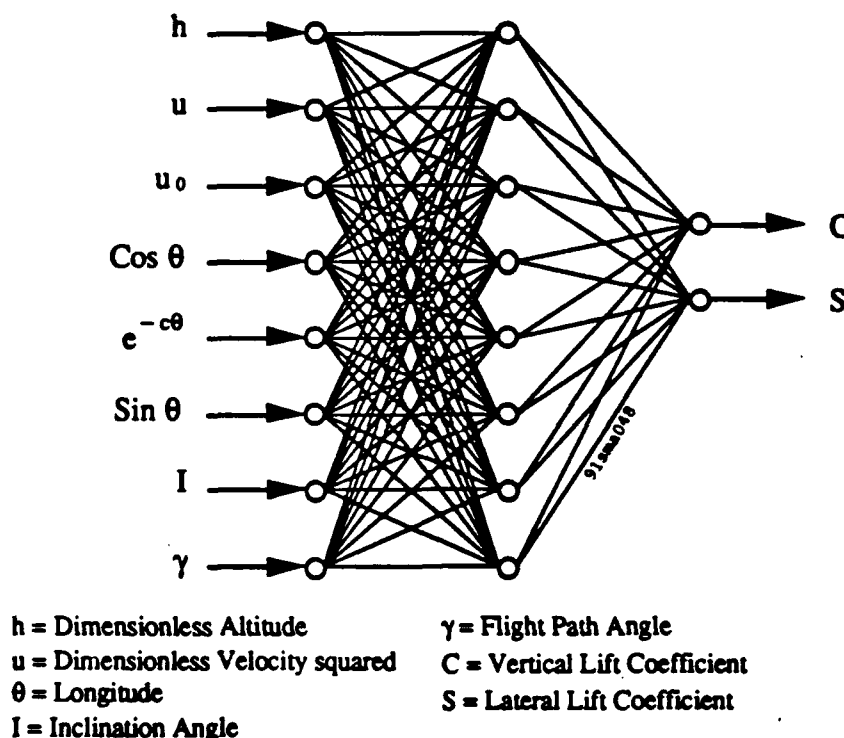


Figure 3-10: I/O Set 1 and a Single Hidden Layer Interconnect Structure

I/O Set 2:

The inputs of I/O Set 2 are derived from the form of the optimal solution to the soft maneuver described by the following (Vinh and Ma (1990b)):

$$C = \frac{E^* \tan \gamma}{k_1 u - 1} \quad (3.3)$$

$$S = \frac{E^* (k_2 \cos \theta + k_3 \sin \theta) \cos \phi}{(k_1 u - 1) \cos \gamma}$$

where k_1 , k_2 , and k_3 are normalized constants and E^* is the maximum lift to drag ratio. Since $\tan \gamma$, $\cos \theta$, $\cos \phi$, and $\cos \gamma$ all have a direct functional relationship to C and S , they will be used as inputs for I/O Set 2. Altitude (h), velocity (u), and initial velocity (u_0) will be used directly as in I/O Set 1. Longitude will also be used directly to give the network temporal information that I/O Set 1 received through the $e^{-c\theta}$ term. Figure 3-11 illustrates I/O Set 2 for a multiple hidden layer network.

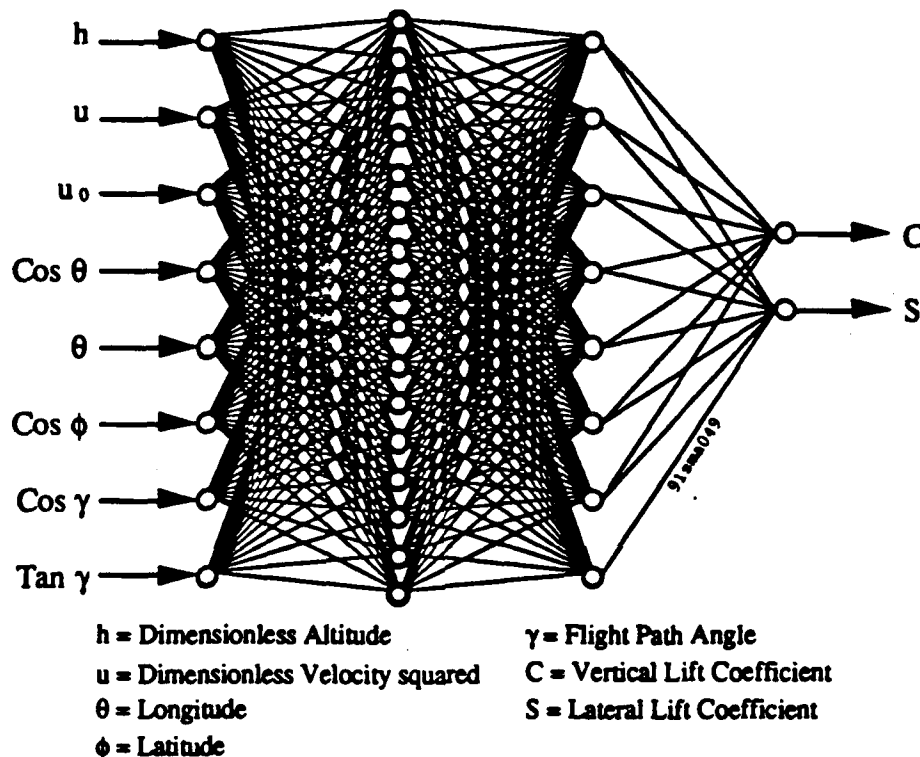


Figure 3-11: I/O Set 2 with a Multiple Hidden Layer Interconnect Structure

Interconnect Structures:

The second step in the neural net modelling of the optimum trajectory database is to define the interconnect structure for the neural guidance network. The approach taken here is to define several different interconnect structures, train them with both I/O sets independently, and evaluate the open- and closed-loop performance of the interconnect structure that produces the smallest RMS training error.

We define two types of interconnect structures: one with a single hidden layer (SHL) and one with multiple hidden layers (MHL). For each type of interconnect structure, the number of nodes in the hidden layer(s) are varied. Table 3-1 shows the defined interconnect structures and the number of nodes in each layer. Four SHL networks are defined with 8, 16, 24, and 32 hidden nodes, respectively. Three MHL networks are

defined each with two hidden layers. These networks have 16, 24, and 32 nodes in their first hidden layer and 8, 12, and 16 nodes in their second hidden layer, respectively.

Table 3-1: Number of Nodes in Network Interconnect Structures

One Hidden Layer	Two Hidden Layers
8-8-2	8-16-8-2
8-16-2	8-24-12-2
8-24-2	8-32-16-2
8-32-2	

All of networks described here are fully connected, i.e., every node in a given layer is connected to each node in the following layer. Figure 3-10 shows a fully connected network with 8 nodes in its single hidden layer. Figure 3-11 shows a fully connected network with 16 nodes in its first hidden layer and 8 nodes in its second hidden layer.

3.3.3 Neural Net Guidance Training

Training and Evaluation Database:

Before training of a defined neural net architecture can begin, a training and open-loop evaluation database must be created. This database is a scaled subset of the optimal guidance trajectory database (described in section 3.3.1). Scaling is necessary because the sigmoid activation function used by the network outputs values between the asymptotic limits of 0 and 1. The neural guidance database is scaled between 0.1 and 0.9 since the asymptotic limits of the sigmoid function are unattainable.

Three sets of optimal trajectories were generated: one set each for $u_0 = 1.3$, $u_0 = 1.45$, and $u_0 = 1.6$. Each trajectory set consists of approximately 360 data points for each orbit, resulting in approximately 2880 data points for the $u_0 = 1.3$ case, 5400 for the $u_0 = 1.45$ case, and 7560 for the $u_0 = 1.6$ case. After scaling, the optimal database is separated into two training and an evaluation databases: one training and evaluation database for I/O Set 1 and one for I/O Set 2.

The training data is a uniform random sample of the $u_0 = 1.3$ and 1.6 trajectories. An average of 10 data points per orbit is selected resulting in 80 training points (I/O pairs) from the $u_0 = 1.3$ data and 210 I/O pairs from the 1.6 data. Figure 3-12 shows the vertical lift coefficient (C) profiles for the training trajectories ($u_0 = 1.3$ and 1.6), where the "♦"s indicate the sampled training data.

The evaluation data to be used in testing the open-loop performance of the defined network architectures is a uniform random sample of the $u_0 = 1.3$, 1.45, and 1.6 data. An average of 36 data points per orbit is selected resulting in about 280 evaluation points from the $u_0 = 1.3$ data, 540 from the 1.45 data, and 756 from the 1.6 data, for a total of 1576 I/O pairs.

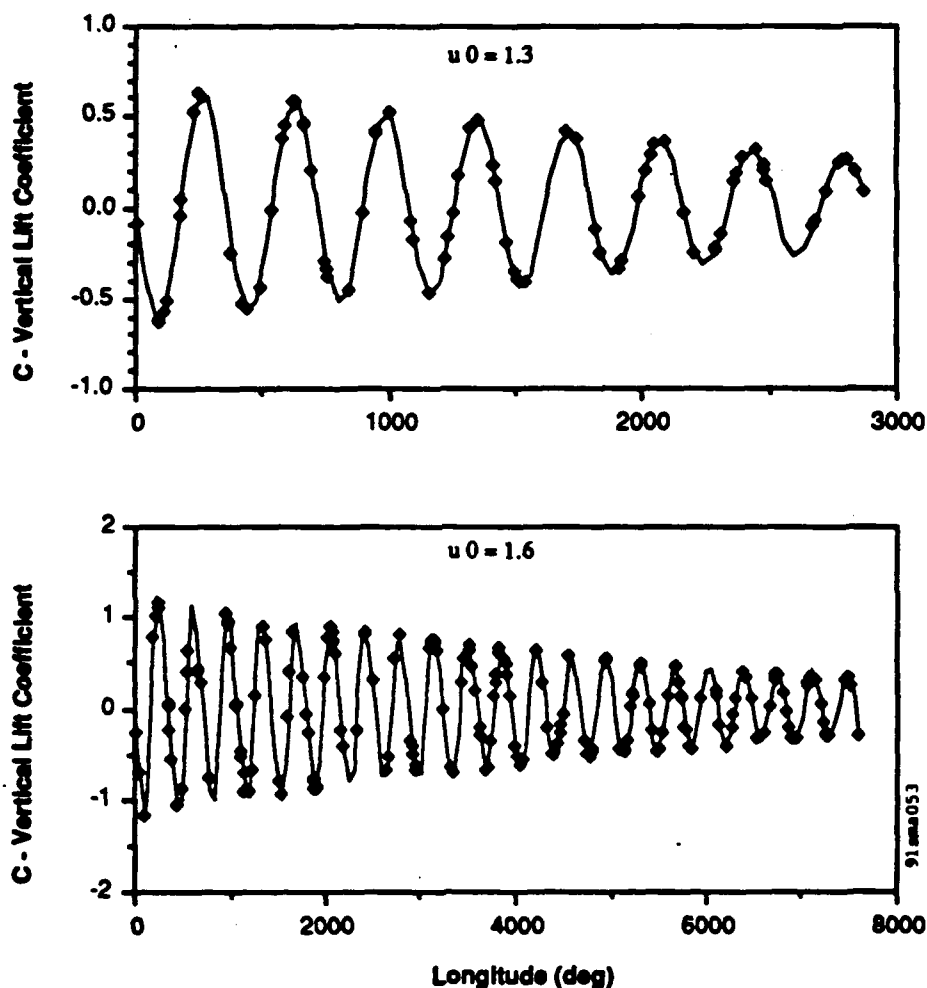


Figure 3-12: C Profiles with Selected Training Data

Training Performance:

Training a network requires cycling the training data through the network and adjusting the connection weights to minimize the output error. During each training cycle all of the 290 IO pairs in the training database are presented to the network. Each SHL network is trained for 10,000 cycles using both I/O Sets. Similarly, each MHL network is trained for 30,000 cycles using both I/O Sets. Here, we discuss the training performance of the network architectures described in section 3.3.2. Training performance is measured in

terms of network output RMS error after a given number of training cycles. The training performance of the four SHL networks is presented followed by the training performance of the three MHL networks.

Single Hidden Layer Network Training Performance:

Figure 3-13 shows the rate at which the various SHL networks learn the functional relationships between the inputs and the outputs of the training data for both I/O Sets. The plotted RMS error is calculated using the scaled errors in both network outputs (C and S) for each training cycle. As is typical with backpropagation networks, the RMS error decreases rapidly at first but then slows as it asymptotes toward a minimum value.

Figure 3-13 (a) compares the training performance of the SHL networks trained on I/O Set 1. After 10,000 cycles, the network with 24 hidden nodes reaches the lowest RMS error (0.0031) and, therefore, performs the best. Conversely, the network with 8 hidden nodes performs the worst with a final RMS error of 0.0048. The 16 and 32 SHL networks achieve similar RMS errors of about 0.0035. For this problem, adding more than 24 hidden nodes does not improve the training performance. A network with 28 hidden nodes (not shown) achieves an RMS error of 0.0034, supporting this observation.

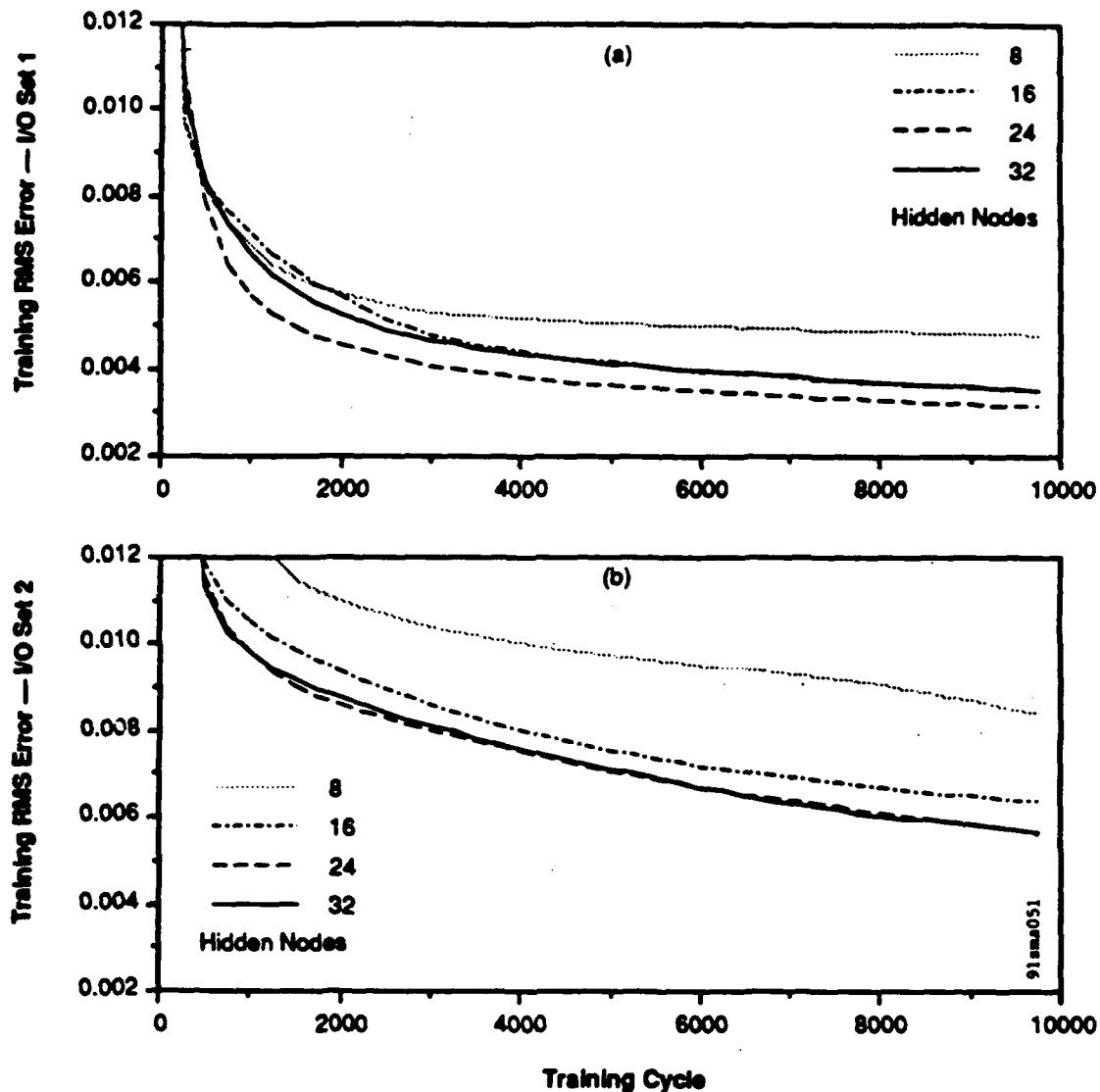


Figure 3-13: Learning Rate of the Single Hidden Layer Networks

Similar results are shown in figure 3-13 (b) for the SHL networks trained on I/O Set 2. Again, the network with 24 hidden nodes reaches the lowest RMS error (0.0055) and the network with 8 hidden nodes performs the worst with a final RMS error of 0.0083. The network with 32 hidden nodes performs almost as well as net 24 in reaching a final RMS error 0.0056, showing once again that adding more than 24 hidden nodes does not improve training performance.

Comparing figure 3-13 (a) with (b) shows that the choice of network inputs has a significant effect on the ability of the various networks to learn the desired outputs (C and S). All of the networks trained on I/O Set 1 achieve lower RMS errors than any of the networks trained on I/O Set 2.

Multiple Hidden Layer Network Training Performance:

In an effort to improve training performance beyond that of the 24 hidden node SHL networks, a second hidden layer is added to the network architecture. Figure 3-14 shows the rate at which the various MHL networks learn the functional relationships between the inputs and the outputs of the training data for both I/O Sets. For reference, the RMS error of the 24 hidden node SHL network is also plotted.

Figure 3-14 (a) compares the training performance of the MHL networks trained on I/O Set 1. After 30,000 cycles, all of the MHL networks reach lower RMS errors than the best performing SHL network. The 32_16 network has the best training performance with a final RMS error of 0.0009. The final RMS errors for the 16_8 and 24_12 MHL networks are 0.0018 and 0.0015, respectively.

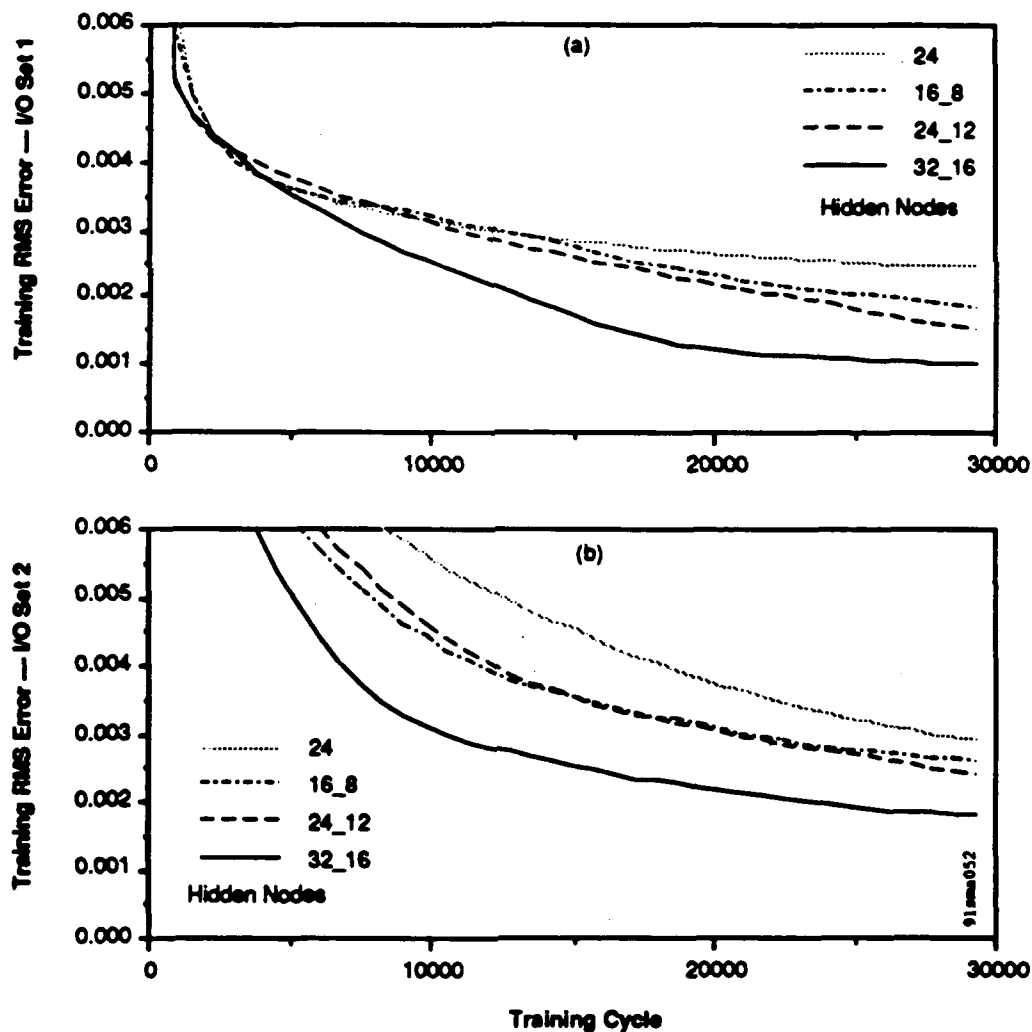


Figure 3-14: Learning Rate of the Multiple Hidden Layer Networks

Similar results are shown in figure 3-14 (b) for the MHL networks trained on I/O Set 2. Again, all of the MHL networks reach lower RMS errors than the best performing SHL network and the 32_16 network has the best training performance with a final RMS error of 0.0017. The final RMS errors for the 16_8 and 24_12 MHL networks are 0.0026 and 0.0024, respectively.

As is the case with the SHL networks, comparing figure 3-14 (a) with (b) shows that the choice of network inputs has a significant effect on the ability of the various networks to learn the desired outputs (C and S). The networks trained on I/O Set 1 achieve lower RMS errors than like networks trained on I/O Set 2.

In summary, there are two main observations to make about the results presented in this section. First, the training performance of a network trained on I/O Set 1 is better than the training performance of the same network trained on I/O Set 2. The inputs selected for I/O Set 1 allow the networks to learn the desired outputs more easily than the inputs selected for I/O Set 2. Second, for a given I/O set, the network with the most complex interconnect structure considered here (MHL 32_16) also has the best training performance. This is not to say that an infinite number of hidden nodes will result in the best training performance. As is the case with the SHL networks, a point will be reached when the addition of more hidden nodes will not improve training performance.

3.3.4 Neural Net Guidance Evaluation

Presented in this section is an evaluation of the open-loop and closed-loop performance of the 32_16 MHL neural guidance network. The performance of this network which was trained on both I/O sets is considered. Open-loop results refer to the performance of the neural guidance network when the evaluation data is propagated through the network and the outputs generated are compared to the corresponding optimum guidance controls. Closed-loop results show the performance of the neural guidance network when it is integrated into the simulation as a feedback guidance law.

Open-Loop Performance:

The open-loop results are generated by presenting the evaluation data to the trained network and comparing the desired outputs to the actual outputs. Recall, from section 3.3.3 that the evaluation data contains 1576 data points; 540 of these points are from the non-training trajectory ($u_0 = 1.45$). Since the evaluation data is chosen at random, the network approximates optimal controls for 1576 sets of vehicle states that were not presented to it during training.

A comparison between the network's training performance and its open-loop performance is shown in figure 3-15. The plotted RMS error is calculated using the same method as the RMS errors discussed in section 3.3.3, that is, the scaled errors in both network outputs (C and S) are used in the calculation. Therefore, the training RMS errors in figure 3-15 are the same as the final RMS errors for the 32_16 MHL network shown in figure 3-14. Note that the RMS error of the evaluation data is higher than that of the training data for both I/O sets. This is expected since the network is not trained using the evaluation data. Also note that the network trained on I/O Set 1 produces a lower evaluation RMS error than the network trained on I/O Set 2. This is also expected, since the I/O Set 1 network trained to a lower RMS value. However, since like networks trained on both I/O sets produce open-loop RMS errors that are less than 0.01 (1.0%), they should both perform well when implemented as neural guidance networks in the closed-loop simulation.

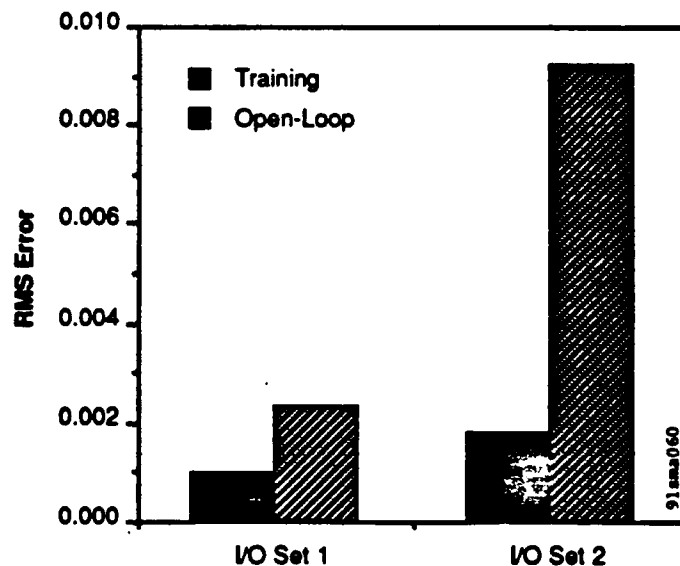


Figure 3-15: Training and Open-Loop Performance Comparison

Although figure 3-15 indicates the overall open-loop performance, analyzing how well the network predicts the individual outputs is also instructive. Figure 3-16 shows the RMS errors in each control (C and S) for the trajectories considered ($u_0 = 1.3, 1.45$, and 1.6). The RMS errors plotted here are calculated using unscaled values of C and S. There are two main features to note about this figure. First, the network has a more difficult time predicting C than it has predicting S, no matter which I/O set the network is trained with. Secondly, for the training trajectories ($u_0 = 1.3, 1.6$), the network trained with I/O Set 1 has smaller C and S RMS errors, then the I/O Set 2 network. However, for the nontraining trajectory ($u_0 = 1.45$), both I/O set networks perform about the same.

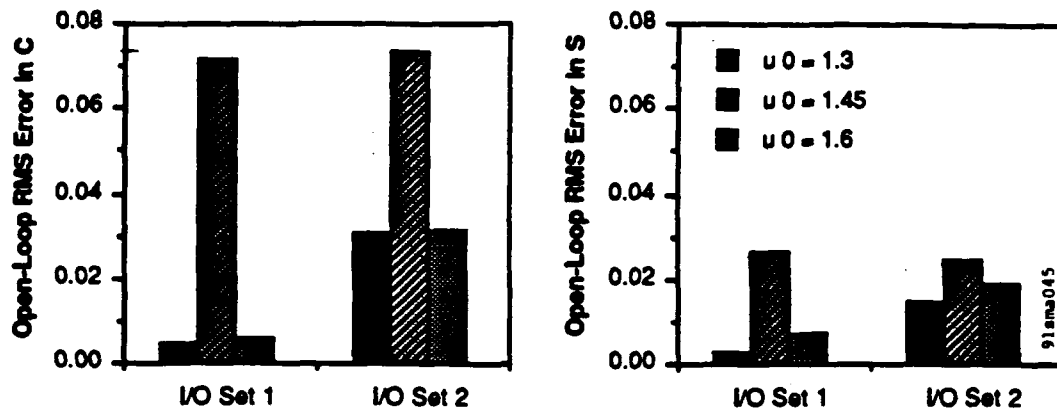


Figure 3-16: Open-Loop Control Performance

Closed-Loop Performance:

Closed-loop results are generated using the simulation described in section 3.3.1 with the trained neural network producing the feedback guidance commands for the $u_0 = 1.3$, 1.45, and the 1.6 set of trajectories. Figure 3-17 compares the performance of the 32_16 MHL network trained on I/O Set 1 data with that of the I/O Set 2 network. This figure shows the unscaled RMS errors in the vehicle controls produced by the neural guidance network, as well as the states resulting from the use of those controls. As is expected from the open-loop results, the network trained on I/O Set 1 consistently produces lower RMS errors for like states and controls than the I/O Set 2 network. The one exception is the control S for the nontraining trajectory, where the I/O Set 2 network has a slightly lower RMS error. However, the I/O Set 1 network still has lower state errors, which implies that predicting C correctly is more important than predicting S correctly.

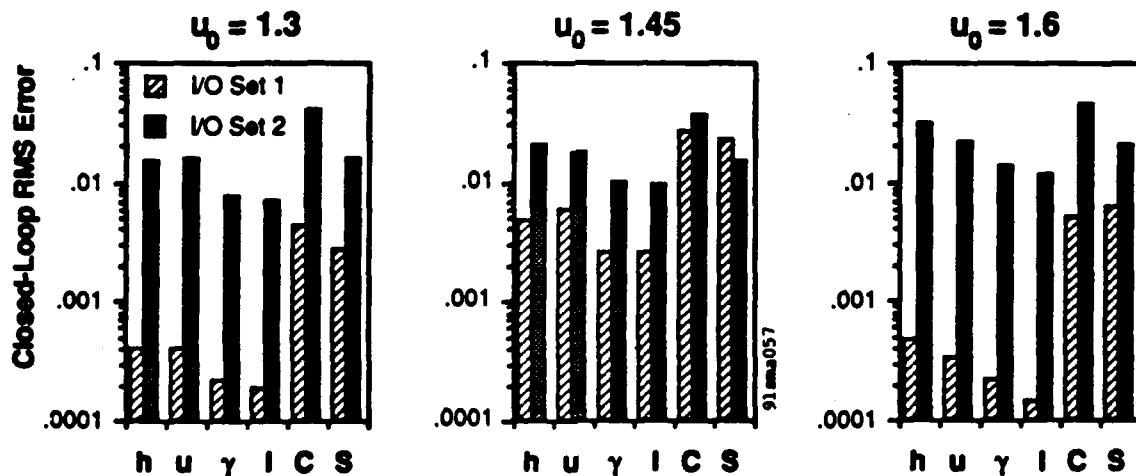


Figure 3-17: Closed-Loop I/O Set Comparison

Figure 3-18 shows the same closed-loop RMS errors, as in figure 3-17, plotted with respect to each I/O Set in order to compare the neural guidance performance between training and nontraining trajectories. Note that the I/O Set 1 network produces relatively large errors for the nontraining trajectory ($u_0 = 1.45$) when compared to errors in the training trajectories ($u_0 = 1.3$ and 1.6). In contrast, the I/O Set 2 network produces more consistent errors across trajectories. In fact, it produces larger errors for the training trajectory of $u_0 = 1.6$, then for the nontraining trajectory.

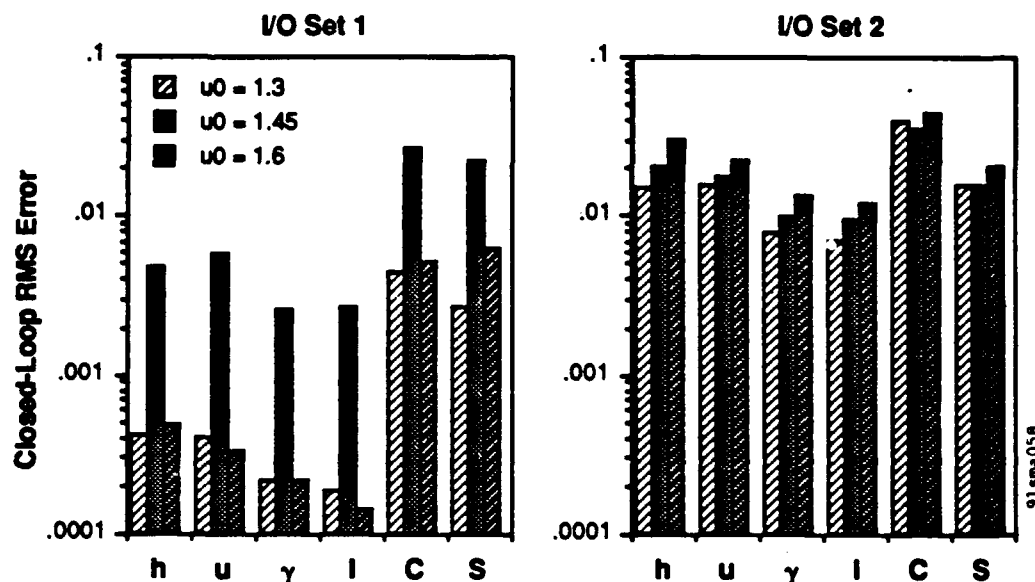


Figure 3-18: Neural Guidance Closed-Loop Performance on the Nontraining Trajectory

Another important measure of performance, besides the state and control RMS errors, is the neural guidance error in the optimized parameter, the final inclination (I_f). Figure 3-19 shows the final inclination and longitude produced by the optimal control law and the two I/O set neural guidance control laws for the three trajectories considered. The stopping criterion for the simulation is circularization of the orbit. Therefore, the values shown in the figure are the current inclination and longitude at the point of a circularization.

As seen in the figure, the I/O Set 1 neural guidance network reaches almost identical values for final inclination and longitude as the optimal control law. For the training trajectories, I/O Set 1 network reaches the same final inclination as the optimal control law and does so at the same final longitude. For the nontraining trajectory, I/O Set 1 misses the final inclination by 0.25° ; an error of 1.6%. For all three trajectories, the I/O Set 2 network reaches the stopping criterion before achieving the final inclination of the optimal control

law. However, the final inclinations it does achieve are within 1.3° of optimal; an error of less than 6.4 %.

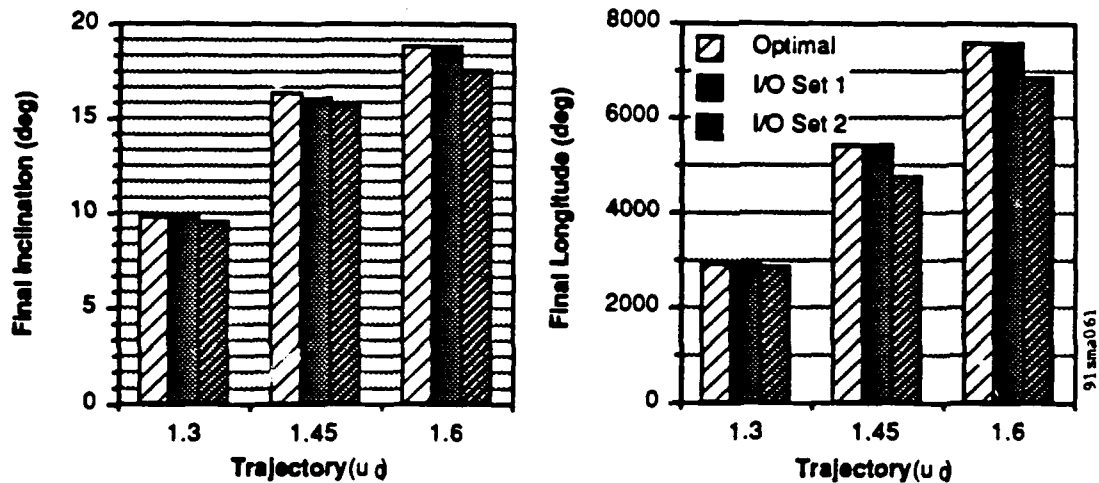


Figure 3-19: Closed-Loop Final Inclination and Longitude

An important consideration in the development of the neural guidance law is the retention of performance in the face of parameter uncertainty. Here, we present the closed-loop performance of the neural guidance network when subjected to a parameter uncertainty. For this demonstration, the 32_16 MHL network, trained on I/O Set 1, is used to predict the controls for the nontraining trajectory ($u_0 = 1.45$) subjected to uncertainty in the maximum lift/drag ratio (E^*). To simulate uncertainty in E^* , filtered white noise is added to the constant value of $E^* = 1.5$ used in the previous closed-loop results. Figure 3-20 shows the profile of the noisy E^* with respect to longitude.

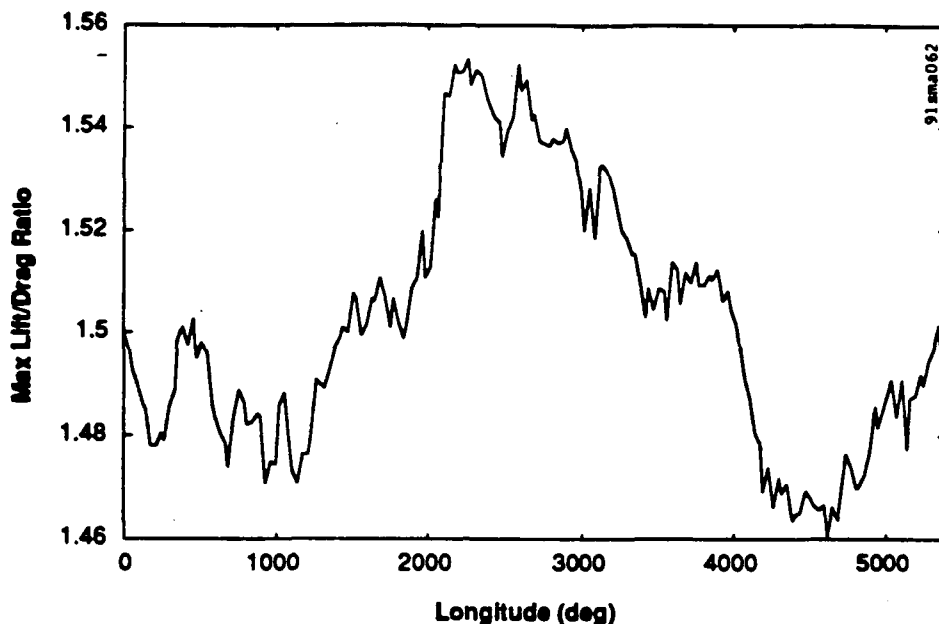


Figure 3-20: Maximum Lift/Drag Ratio with Noise ($u_0 = 1.45$)

Figure 3-21 shows the control histories generated using the optimal control law subjected to the uncertainty in E^* . The trajectory terminated prematurely, as shown in the figure, due to numerical integration errors arising from the random fluctuation in E^* . In contrast, the neural guidance law performs exceptionally well when subjected to the uncertainty introduced into E^* . The control histories generated using the neural control law under parameter uncertainty, as shown in figure 3-22, complete the desired orbital maneuver.

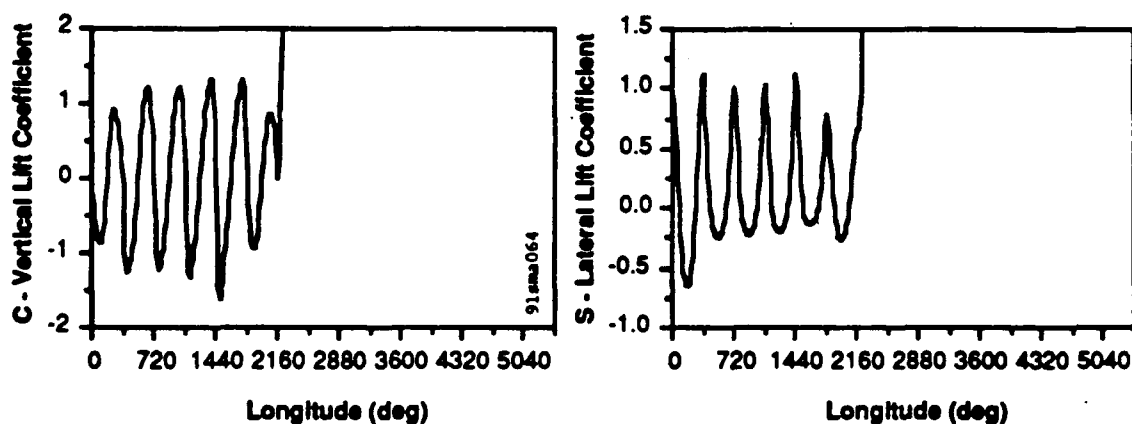


Figure 3-21: Optimal Control Performance Under Parameter Uncertainty

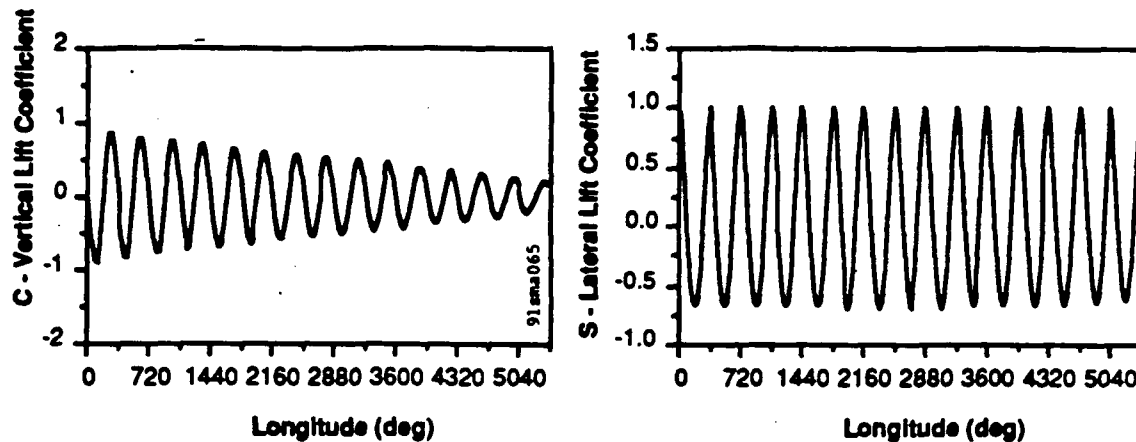


Figure 3-22: Neural Control Performance Under Parameter Uncertainty

The best measure of closed-loop control law performance is how well the control law achieves its objective, in this case maximizing final inclination. Figure 3-23 compares the final inclinations and longitudes of the optimal control law with and without E^* uncertainty and the I/O Set 1 neural guidance law with and without E^* uncertainty. Whereas the parameter uncertainty causes the optimal control law to terminate prematurely resulting in a low value of final inclination, the neural control law with parameter uncertainty reaches a final inclination value comparable to the trajectories generated without parameter uncertainty. These results demonstrate that the developed neural control law is robust to uncertainty in spacecraft parameters such as E^* .

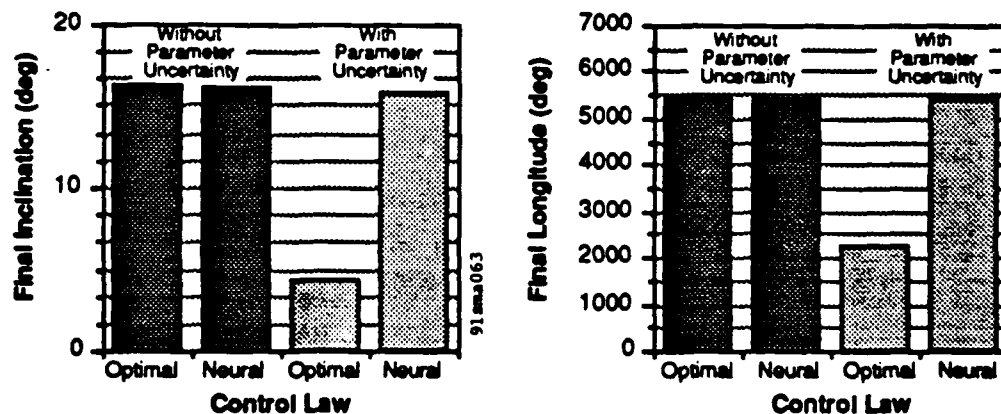


Figure 3-23: Closed-Loop Control Law Performance Under Parameter Uncertainty

3.4 Feasibility Assessment of Neural Net Guidance

We have presented in this chapter a neural net approach to deriving closed-loop LightSat/TacSat AOT guidance laws. In the developed approach, several neural network interconnect structures are trained off-line with a database of guidance/trajectory solutions

computed using a numerical optimization algorithm. The neural guidance architectures are developed using the backpropagation neural network paradigm because this paradigm is well suited for input to output mapping required to model the optimum guidance solution. The computed optimal trajectory database contains three separate trajectories for the multi-pass plane change maneuver. Using a priori knowledge about the optimal solution, two sets of inputs/output training databases are generated from two of the optimal trajectories. The third optimal trajectory is used for open- and closed-loop evaluation of the trained neural guidance law. Seven different interconnect structures are trained using the two training databases.

The results presented in section 3.3 demonstrate the feasibility of developing a neural guidance network to generate on-line guidance commands with an acceptable level of error, even in the presence of parameter uncertainty. In particular, a backpropagation neural network can be trained to model the optimal guidance solution for a maximum inclination change multi-pass plane change maneuver. The performance of the neural guidance law closely matches that of the optimal guidance law. In the absence of parameter uncertainty, for the three trajectories considered ($u_0 = 1.3, 1.45, 1.6$), the neural guidance law has a maximum error in final inclination of 1.6%. In the presence of parameter uncertainty, for the nontraining trajectory ($u_0 = 1.45$), the neural guidance law outperforms the optimal guidance law. The training trajectories are not considered since the nontraining trajectory represents the worst case. When using the optimal control law, the simulation with a noisy E^* terminates execution prematurely due to failure of the control law. However, when using the neural guidance law, a final inclination is reached that is only 3.5% off of the non-noisy optimal solution.

4. Summary, Conclusions, and Recommendations

4.1 Summary

Our general technical approach to evaluate alternative aeroassisted orbital transfer concepts and to demonstrate feasibility of an on-line neural network implementation of an atmospheric trajectory/guidance scheme centers on: 1) identification of aeroassisted orbital transfer concepts applicable to the LightSat/TacSat community; 2) the performance of trade studies to evaluate feasibility of these concepts and to determine key concept design drivers; 3) formulation and evaluation of neural network implementation for a given AOT trajectory/guidance database; and 4) propose follow-on design objectives and development paths for a specific LightSat/TacSat implementation and validation effort.

The first step in researching alternative aeroassisted orbital transfer concepts is the identification of all possible functional uses of such concepts. This requires the determination of vehicle/mission elements that may be enhanced through the use of aeroassisted maneuver concepts. Consideration is given to classifying the types of vehicles/missions that are or could be capable of aeroassisted maneuvers (e.g., small satellites in LEO, reconnaissance spacecraft in Molniya orbits, or polar sun synchronous satellites). Next, for these vehicles a determination of how can aeroassisted maneuvers enhance or augment mission effectiveness or prolong mission lifetime is required. This involves identifying specific mission orbital requirements, i.e., inclination stationkeeping, perigee location, satellite relocation, etc. Finally, the satellite parameters that play key roles evaluating feasibility of AOTs are identified.

The second step in this research effort is the performance of trade studies to determine the overall design drivers. Included in these studies is the analysis of both vehicle configuration/constraints and overall mission requirements. For a given concept and satellite, we look at the vehicle characteristics such aerodynamic coefficients, mass properties, physical characteristics, etc. Also studied are performance benefits obtained including enhanced mission effectiveness, increased mission lifetime, etc.

The third step of our effort is the formulation and evaluation of neural network architectures for an AOT guidance concept. In particular, various interconnect architectures and processing elements will be considered to incorporate the known attributes of the optimum guidance solution. The networks are trained on trajectories developed and then are evaluated on its on-line performance in classifying the optimum trajectories, approximating

the optimal solution, satisfying end conditions, and coping with environmental uncertainties.

4.2 Conclusions

The primary results of this study are the identification of possible new applications of aeroassisted orbital transfers to LightSat/TacSats and the feasibility evaluation of an on-line neural network implementation of an atmospheric trajectory/guidance scheme. The major findings of this effort are summarized in the following paragraphs.

AOT scenarios can be classified into 2 distinct categories: on-orbit multiple-pass "soft maneuvers" and the single-pass deep penetration into the atmosphere "hard maneuver". Due to propellant limitations, the soft maneuver is very conducive to address LightSat/TacSat orbital transfer requirements. Possible soft-maneuvers include inclination and perigee location stationkeeping. Hard maneuvers are more conducive to situations requiring a greater amount of maneuverability, e.g., emergency relocation of a satellite.

Associated with each class of AOTs are a set of relevant vehicle and mission requirement parameters. This set of parameters help define the overall feasibility of AOTs. Chief among these parameters is perigee altitude. Perigee altitude determines the amount of atmospheric density available to perform on-orbit maneuvers. Density is seen to decrease exponentially with altitude such that AOTs are not feasible beyond a perigee altitude of 200 km. Lower perigee altitudes come with a detrimental effect of shorter orbital lifetimes. This can be ameliorated via more eccentric orbits. Among the relevant vehicle parameters are satellite mass, reference area, and aerodynamic efficiency.

Trade studies were performed for two specific soft maneuvers: plane change and rotation of line of apsides. Approximate sub-optimal expressions for plane change and apsidal rotation per revolution were derived. Parameters of interest were then varied with the following results:

- Variation of perigee height shows orders of magnitude increase in maneuver capability per revolution when going from 200 km to a 100 km perigee height due to increasing atmospheric density. Such an increase in maneuver capability is offset by the low orbital lifetimes at such altitudes, especially for low eccentricities.
- The amount of plane change and apsidal rotation per revolution decreases with increasing eccentricity. However, higher eccentricity has a beneficial effect on

on-orbit lifetime. The decrease in plane change is by a factor of two over the eccentricity range of 0.1 to 0.6 with lifetime increasing by an order of magnitude from about 10 days to almost one year. Apsidal rotation per revolution decreases initially with increasing eccentricity, as with plane change, but then flattens out at higher eccentricities while lifetime increases. Higher eccentricity orbits not only have a longer lifetime, but over the total lifetime achieved a greater total amount of plane change and apsidal rotation.

- An increase in satellite reference area has a beneficial effect on plane change and apsidal rotation per revolution while orbital lifetime is decreased. Since reference area linearly increases maneuver amount and linearly decreases orbital lifetime, the total maneuver amount over the lifetime is constant over the range of reference area with all other parameters held fixed.
- Mass decreases plane change and apsidal rotation per revolution with a concomitant beneficial effect on orbital lifetime. Lower mass, while producing a greater plane change and rotation per revolution, comes with lower lifetime cost, that is, a greater amount of maneuver is accomplished faster with smaller masses but with total orbital change over lifetime equal for all masses.
- Variation of vehicle aerodynamic coefficients with altitude were accomplished via exponential curve fits to common values encountered at perigee heights of 200 and 100 km. As a function of perigee height, results show orders of magnitude decrease in plane change and apsidal rotation per revolution with increasing altitude due to density and lift coefficient reduction. The results are comparable with those presented on perigee height variation with the superimposition of the effect of aerodynamic coefficient variation. These results further the necessity for performing maneuvers at lower altitudes.

Two AOT scenarios have demonstrated feasibility based on results of the trade studies. These are the inclination and rotation of line of apsides on-orbit stationkeeping maneuvers. For a 25 kg satellite with a perigee height of 150 km and an eccentricity of 0.6, a total lifetime plane change of over 3 degrees and a total apsidal rotation of over 5 degrees were demonstrated. Plane changes of 20° and higher become possible for lower perigee heights and with more aerodynamical efficient satellites. Possible applications of these maneuvers include stationkeeping for a satellite with a near-equatorial perigee location or compensating for rotating argument of perigee for satellites at near Molniya orbits. Other possible AOT

scenarios include orbit circularization via the multi-pass maneuver, and the controlled deorbit of a satellite to prolong orbital lifetime or to relocate the satellite to deorbit over a strategic geographic region.

We have generalized our neural guidance approach to deriving closed-loop LightSat/TacSat AOT guidance laws. Several neural network interconnect structures were trained off-line with a database of guidance/trajectory solutions computed using a numerical optimization algorithm. The known characteristics of the optimal solution were used to determine two sets of network inputs and outputs. The on-line realization of the trained neural guidance laws generates the real-time guidance commands based on current measurements and initial constraints. The training, open-loop, and closed-loop performance of the neural guidance networks were evaluated with the following results:

- A backpropagation neural network can be trained to model the optimal guidance solution for the multi-pass plane change maneuver. The performance of the neural guidance law closely matches that of the optimal guidance law. In the presence of parameter uncertainty, the neural guidance law outperforms the optimal guidance law.
- A priori knowledge about the optimal solution can be incorporated into the neural network architecture. Networks with like interconnect structures trained to acceptable levels using the two different sets of inputs/outputs.
- Choice of network inputs impacts the rate at which the network learns the functional relationships required to predict the desired control commands. One set of inputs/outputs consistently produced better training performance over all network interconnect structures than the other set of inputs/outputs.
- For the multi-pass plane change maneuver, a multiple hidden layer network learns the desired controls faster than a single hidden layer network. For either input/output set, a given multiple hidden layer network reached a lower RMS error in a fewer number of training cycles than a given single layer network.

4.3 Recommendations

We recommend a development of a real-time demonstration of a neural network controller for a LightSat/TacSat aeroassisted orbital transfer maneuver. A three part design and demonstration program under a Phase II effort is required:

- Identification and definition of a realistic feasible AOT applicable to the LightSat/TacSat community. The purpose here would be to glean from the Phase I results an AOT most conducive for implementation. Specific tasks include determination of the optimal control strategy, neural network architecture definition and training, controller actuation requirements, overall controller hardware and software requirements, and subsystem interface requirements.
- Development of real-time design demonstration to emulate the on-orbit performance of a neural guidance system for the chosen LightSat/TacSat AOT. The effort would entail the evaluation of the functional performance of such a system in terms of: accuracy of orbital transfer; robustness of neural controller to disturbances (e.g., random fluctuations in density); and real-time operational requirements of neural controller within the constraints on current digital microprocessors, satellite imposed constraints, and satellite subsystem interface options. The objective here is to critically evaluate the feasibility of neural guidance for an AOT and assess its potential for meeting the actual on-orbit objectives.
- Definition of a follow-on effort to design an actual on-orbit experiment. This would entail a detailed design effort to piggy-back the AOT neural network controller system on an existing or future DARPA LightSat/TacSat. A detailed interface requirements analysis would be performed to determine possible interaction of the system with the onboard subsystems (e.g., power requirements, data handling/processing, telemetry, etc.).

5. References

- Baffes, P.T. 1989. *NETS User's Guide*. Software Technology Branch, Lyndon B. Johnson Space Center.
- COSPAR. 1972. *COSPAR International Reference Atmosphere*. Berlin: Akademie-Verlag.
- Gur, I., Mishne, D. and Taratuta, A. 1990. "Multipass Aeroassisted Transfer Between Coplanar Elliptical Orbits in the Presence of Atmospheric Density Variations." *AIAA Flight Mechanics Conference*.
- Halyo, N. and Taylor, D.B. 1989. *Optimal Aeroassisted Coplanar Orbital Transfer Using an Energy Model*. NASA. CR-181778.
- Hecht-Nielsen, R. 1991. *Neurocomputing*. Reading, MA: Addison-Wesley.
- Hull, D.G., Giltner, J.M., Speyer, J.L., et al. 1985. "Minimum Energy-Loss Guidance for Aeroassisted Orbital Plane Change." *J. Guidance*, Vol. 8, No. 4: 487-493.
- Ikawa, H. 1986. "A Unified Three-Dimensional Trajectory Simulation Methodology." *Journal of Guidance and Control*, Vol. 9, No. 6.
- King-Hele, D.G. 1987. *Satellite Orbits in An Atmosphere: Theory and Applications*. Glasgow, Scotland: Blackier and Son Ltd.
- Rumelhart, D.E. and McClelland, J.L. 1988. *Parallel Distributed Processing*. Cambridge, MA: The MIT Press.
- Vinh, N.X. and Johannesen, J.R. 1986. "Optimal Aeroassisted Transfer Between Coplanar Elliptical Orbits." *Acta Astronautica*, Vol. 13, No. 6/7: 291-299.
- Vinh, N.X. and Ma, D. 1990a. "Optimal Multiple-Pass Aeroassisted Plane Change." *Acta Astronautica*, Vol. 21, No. 11/12: 749-758.
- Vinh, N.X. and Ma, D. 1990b. "Optimal Plane Change By Low Aerodynamic Forces." *AIAA Flight Mechanics Conference*.
- Walberg, G.D. 1985. "A Survey of Aeroassisted Orbit Transfer." *Journal of Spacecraft and Rockets*, Vol. 22, No. 1.
- Wertz, J.R., ed. 1985. *Spacecraft Attitude Determination and Control*. Boston, MA: D. Reidel Publishing Co.
- Wertz, J.R. and Larson, W., J. 1991. *Space Mission Analysis and Design*. Dordrecht, Netherlands: Kluwer Academic Publishers.

Appendix A: Related Bibliography

A.1 Plane Change Maneuvers

- Hougui, S. and Mishne, D. 1990. "An Approximate Guidance Law for Atmospheric Plane Change Maneuver of an Aerocruise Space Vehicle." *AIAA Flight Mechanics Conference*.
- Hsu, F.-K. and Kuo, T. 1990. "Optimal Aeroassisted Orbital Plane Change with Heating-Rate Constraint." *J. Guidance*, Vol. 13, No. 1: 186-189.
- Hull, D.G. 1985. "New Analytical Results for AOTV Guidance." *AIAA Atmospheric Flight Mechanics Conference*. Snowmass, CO.
- Hull, D.G., Giltner, J.M., Speyer, J.L., et al. 1985. "Minimum Energy-Loss Guidance for Aeroassisted Orbital Plane Change." *J. Guidance*, Vol. 8, No. 4: 487-493.
- Hull, D.G. and Speyer, J.L. 1982. "Optimal Reentry and Plane-Change Trajectories." *Journal of the Astronautical Sciences*, Vol. 30, No. 2: 117-130.
- Johannesen, J.R., Vinh, N.X. and Mease, K.D. 1985. *Effect of Maximum Lift to Drag Ratio on Optimal Aeroassisted Plane Change*. 85-1817.
- Lee, J.Y. and Hull, D.G. 1990. "Maximum Orbit Plane Change with Heat-Transfer-Rate Considerations." *J. Guidance*, Vol. 13, No. 3: 492-497.
- London, H.S. 1961. "Change of Satellite Orbit Plane by Aerodynamic Maneuvering." *IAS 29th Annual Meeting*. New York. Institute of the Aerospace Sciences.
- McEneaney, W.M. 1991. "Optimal Aeroassisted Guidance Using Loh's Term Approximations." *J. Guidance*, Vol. 14, No. 2: 368-376.
- Naidu, D.S. 1991. "Fuel-Optimal Trajectories of Aeroassisted Orbital Transfer with Plane Change." *IEEE Transactions on Aerospace and Electronic Systems*, Vol. 27, No. 2: 361-369.
- Speyer, J.L. and Crues, E.Z. 1990. "An Approximate Atmospheric Guidance Law for Aeroassisted Plane Change Maneuvers." *Journal of Guidance and Control*, Vol. 13, No. 5.
- Speyer, J.L. and Crues, E.Z. 1990. "Approximate Optimal Atmospheric Guidance Law for Aeroassisted Plane-Change Maneuvers." *J. Guidance*, Vol. 13, No. 5: 792-802.
- Speyer, J.L. and Womble, M.E. 1971. "Approximate Optimal Atmospheric Entry Trajectories." *J. Spacecraft*, Vol. 8, No. 11: 1120-1125.
- Vinh, N.X. and Ma, D. 1990a. "Optimal Multiple-Pass Aeroassisted Plane Change." *Acta Astronautica*, Vol. 21, No. 11/12: 749-758.
- Vinh, N.X. and Ma, D. 1990b. "Optimal Plane Change By Low Aerodynamic Forces." *AIAA Flight Mechanics Conference*.

A.2 Co-Planar Maneuvers

- Gur, I., Mishne, D. and Taratuta, A. 1990. "Multipass Aeroassisted Transfer Between Coplanar Elliptical Orbits in the Presence of Atmospheric Density Variations." *AIAA Flight Mechanics Conference*.
- Karasopoulos, H.K. and Norris, R.B. *Noncoplanar Orbit Transfer Optimization for an Aeroassisted Sortie Vehicle*. Wright-Patterson AFB.
- Lee, B. and Grantham, W.J. 1989. "Aeroassisted Orbital Maneuvering Using Lyapunov Optimal Feedback Control." *J. Guidance*, Vol. 12, No. 2: 237-242.
- Mease, K.D. and Vinh, N.X. 1985. "Minimum-Fuel Aeroassisted Coplanar Orbit Transfer Using Lift-Modulation." *J. Guidance*, Vol. 8, No. 1: 134-141.
- Mishne, D., Melamed, N. and Shinar, J. 1990. "Aeroassisted Transfer Between Elliptical Orbits Using Lift Control." *J. Guidance*, Vol. 13, No. 5: 785-791.
- Naidu, D.S., Hibey, J.L. and Charalambous, C. 1990. "Fuel-Optimal Trajectories for Aeroassisted Coplanar Orbital Transfer Problem." *IEEE Transactions on Aerospace and Electronic Systems*, Vol. 26, No. 2: 374-381.
- Park, C. and Davies, C.B. 1989. "Aerothermodynamics of Sprint-Type Manned Mars Missions." *27th Aerospace Sciences Meeting*. Reno, Nevada.
- Vinh, N.X. and Johannesen, J.R. 1986. "Optimal Aeroassisted Transfer Between Coplanar Elliptical Orbits." *Acta Astronautica*, Vol. 13, No. 6/7: 291-299.

A.3 Miscellaneous

- Caglayan, A.K. and Allen, S.M. 1990. "A Neural Net Approach to Space Vehicle Guidance." *American Control Conference*. San Diego, CA.
- Chern, J.-S., Yang, C.-Y. and Sheen, J.-J. 1988. "Optimal Lift and Bank Modulations for Three-Dimensional Reentry Trajectories with Heat Constraint." *Acta Astronautica*, Vol. 17, No. 3: 303-309.
- Davies, C.B. and Park, C. 1985. "Aerodynamics of Generalized Bent Biconics for Aero-Assisted, Orbital-Transfer Vehicles." *Journal of Spacecraft and Rockets*, Vol. 22, No. 2: 104-111.
- Davies, C.B. and Park, C. 1986. "Aerodynamic and Thermal Characteristics of Modified Raked-Off Blunted Cone." *AIAA/ASME 4th Joint Thermophysics and Heat Transfer Conference*. Boston, MA.
- de Lafontaine, J. 1990. "Orbital Dynamics in a Stochastic Atmosphere." *J. Guidance*, Vol. 13, No. 3: 483-491.
- Gamble, J.D. and Findlay, J.T. 1988. "Shuttle-Derived Densities in the Middle Atmosphere." *AIAA Flight Mechanics*. NASA.
- Ikawa, H. 1985. "A Unified Three-Dimensional Trajectory Simulation Methodology." *AIAA 12th Atmospheric Flight Mechanics Conference*. Snowmass, CO. American Institute of Aeronautics and Astronautics, Inc.

- Ikawa, H. 1988. "Effect of Rotating Earth for Analysis of Aeroassisted Orbital Transfer Vehicles." *J. Guidance*, Vol. 11, No. 1: 47-52.
- Park, C. 1987. "A Survey of Aerobraking Orbital Transfer Vehicle Design Concepts." *AIAA 25th Aerospace Sciences Meeting*. Reno, Nevada. American Institute of Aeronautics and Astronautics.
- Walberg, G.D. 1985. "A Survey of Aeroassisted Orbit Transfer." *J. Spacecraft*, Vol. 22, No. 1: 3-18.